Sequence of rifting in Afar, Manda-Hararo rift, Ethiopia, 2005–2009: Time-space evolution and interactions between dikes from interferometric synthetic aperture radar and static stress change modeling

R. Grandin,[1,2] A. Socquet,[1] E. Jacques,[1] N. Mazzoni,[1] J.-B. de Chabalier,[1,3] and G. C. P. King[1]

Received 21 December 2009; revised 5 July 2010; accepted 28 July 2010; published 16 October 2010.

[1] Thirteen dike intrusions in the Manda Hararo rift, Afar (Ethiopia), from September 2005 to June 2009, studied using an extensive interferometric synthetic aperture radar (InSAR) data set, provide insight into the mechanics of a major active rift. Kinematic inversions of InSAR data reveal that dikes opened by 0.8–3.5 m at an average 5 km depth, with volumes of 0.04–0.2 km^3 (with up to 12 m opening and a volume greater than 1 km^3 for the September 2005 megadike). Dikes have their source in a midsegment magma reservoir, which induces a local shallowing of the brittle-ductile boundary, presumably due to thermal weakening of the lithosphere. The smaller dikes in 2006–2009 were emplaced in regions of minimum opening of the September 2005 megadike, above the central magma reservoir. In contrast, the most voluminous dike intrusions in 2006–2009 occurred near the locus of the peak of maximum opening of the September 2005 megadike, ~10 km north of the magma source. This may suggest that tension on the plate boundary was highest there, both prior to 2005 and possibly also after 2005. Evolution and distribution of normal stress on the plate boundary throughout the rifting episode may indicate that tension near to the magma reservoir is lower than toward segment ends. Average relief of normal stresses of tectonic origin coeval to dike intrusions is comparable with shear stress drops for earthquakes, presumably because dikes in the Manda Hararo rift are intruded at low magma pressure and high tectonic stress.

Citation: Grandin, R., A. Socquet, E. Jacques, N. Mazzoni, J.-B. de Chabalier, and G. C. P. King (2010), Sequence of rifting in Afar, Manda-Hararo rift, Ethiopia, 2005–2009: Time-space evolution and interactions between dikes from interferometric synthetic aperture radar and static stress change modeling, *J. Geophys. Res.*, *115*, B10413, doi:10.1029/2009JB000815.

1. Introduction

[2] Near the Earth's surface (0–20 km depth range), the rheology of rock is elastic-brittle, implying that relative plate motion is discontinuous in time. Earthquakes are spectacular examples of an unstable behavior of slip on faults, and their ubiquity in regions of active tectonics has attracted much attention. Like large earthquakes, dike intrusions may be capable of relieving a significant fraction of the stresses accumulated along a divergent plate boundary by slow motion of tectonic plates, and thus deserve to be considered as major plate boundary events.

[3] A long-standing debate is whether magma-assisted rifting is more efficient than tectonic faulting to allow a continent to break [e.g., *Buck et al.*, 2005]. The two modes of rifting (normal faulting or dike intrusion) share many analogies. For instance, factors controlling the fracture of host rock during a dike intrusion belong partly to the domain of solid mechanics [e.g., *Pollard and Segall*, 1987], as does the problem of earthquake rupture [e.g., *Kostrov and Das*, 1988]. Moreover, dike intrusions are often clustered in time, forming rifting episodes that can last for several years and that are separated by hundreds of years of quiescence. This temporal pattern is referred to as the magmato-tectonic cycle, by analogy with the seismic cycle [e.g., *Björnsson*, 1985].

[4] However, unlike during an earthquake (at least to the first order), the unstable rupture process in operation during a dike intrusion involves a complex interplay between fluid dynamics and fracture mechanics. Indeed, dike intrusions cannot occur spontaneously because an input of magma is required to fill the crack and sustain its propagation [e.g., *Weertman*, 1971]. In the magmatic rifts that constitute the lowest order of segmentation of the mid-ocean ridge system, the source of magma is commonly a reservoir in the center

[1]Institut de Physique du Globe de Paris, Laboratoire de Tectonique et Mécanique de la Lithosphère, Paris, France.
[2]Now at Laboratoire de Géologie, École Normale Supérieure, Paris, France.
[3]Observatoire Volcanologique et Sismologique de Guadeloupe, Gourbeyre, Guadeloupe.

0148-0227/10/2009JB000815

of the segment, and dikes are observed to propagate laterally away from this reservoir [e.g., *Brandsdöttir and Einarsson*, 1979; *Smith and Cann*, 1999; *Dziak et al.*, 2004]. This explains why theoretical and field studies have suggested that a large number of parameters may play an important role during the emplacement of a dike. These include evolution of the internal pressure of the source reservoir, conditions for rupture of magma reservoir walls and dike nucleation, size of the magma chamber, nature and location of magma pathways, surrounding thermal setting, time required for previous dike bodies to solidify, resistance to the flow of magma from the source reservoir to the crack tip, caused by the combined effects of the viscosity of the magma and the small (and variable) section of the conduit, and competition between dike widening and magma freezing [e.g., *Bruce and Huppert*, 1989; *Takada*, 1989; *Lister and Kerr*, 1991; *Rubin*, 1995; *Mériaux and Jaupart*, 1995; *Fialko and Rubin*, 1998; *McLeod and Tait*, 1999]. Unfortunately, few observations are available to constrain complex models of dike intrusions, particularly those addressing the dynamic problem.

[5] The beginning of a major rifting episode in Ethiopia in 2005 represents an invaluable opportunity to provide new insights into the mechanics of dike injection in a magmatic rift. In this paper, we focus on a sequence of dike intrusions that have occurred from September 2005 to June 2009 in the Manda Hararo–Dabbahu rift, in the Afar magmatic province. This rifting episode is the most important ever documented because of its duration (more than 4 years), the large number of dike intrusions (13, at the time of writing), their magnitude (a total of more than 2 km^3 of magma was involved in these intrusions), and the overall length of the rift segment affected by dike intrusions (~65 km) [*Wright et al.*, 2006; *Yirgu et al.*, 2006; *Ayele et al.*, 2007; *Rowland et al.*, 2007; *Ebinger et al.*, 2008; *Keir et al.*, 2009; *Hamling et al.*, 2009; *Grandin et al.*, 2009; *Ayele et al.*, 2009; *Nooner et al.*, 2009; *Grandin et al.*, 2010]. Although the dynamics of dike emplacement throughout the rifting episode is poorly resolved because data are sparse, the static surface displacements induced by each dike can be inferred with great accuracy thanks to satellite geodesy.

[6] Our first objective is to study in detail the succession of dikes in time and space during this sequence, and to understand what controls this organization. To constrain the location and shape of the dikes, we rely on interferometric synthetic aperture radar (InSAR), which, due to the dry and stable climate of Afar, is an efficient geodetic technique that enables us to measure surface displacements with a resolution of a few centimeters, over areas of hundreds of square kilometers [e.g., *Simons and Rosen*, 2007]. Assuming an elastic behavior of the lithosphere during dike injections, InSAR data are inverted to determine the opening distribution of each dike within the sequence. The results of these inversions are then exploited to deduce simple relationships between geometrical and kinematic features of the dikes. We also propose a comparison with magnitude-length scaling laws for tectonic earthquakes involving similar amounts of energy release.

[7] In a second step, we apply simple mechanical modeling to understand how nearby dikes can influence each other. We treat dikes as cracks in an elastic half-space and compute static stress change induced by each dike. This approach, in the case of tectonic earthquakes, has led to the conclusion that earthquakes tend to occur preferentially in areas where Coulomb stress has increased as a result of previous earthquakes [e.g., *King*, 2007]. By analogy, in the case of the rifting episode of Manda Hararo rift, we focus on the evolution of normal stress on the plate interface after each additional dike injection in the sequence, to infer the spatial and temporal evolution of stress on the plate boundary. We focus in particular on the link between the dikes and the mid-segment magma reservoir considered to have fed them. We show that, despite the complexity of the physics describing dike intrusion dynamics mentioned above, a simple model of static stress transfer provides insights into the interaction between dikes. Finally, we discuss implications for the stress conditions on the segment of the plate boundary affected by dike intrusions.

2. Manda Hararo–Dabbahu Rifting Episode

[8] The Manda Hararo–Dabbahu rifting episode (Afar, Ethiopia) initiated in a rift segment showing an early stage of seafloor spreading, which, together with the Asal rift, had previously been recognized as one of the most advanced in the process of oceanization that has been affecting the hot spot-influenced Afar triple point for nearly 30 Ma (Figure 1a) [e.g., *Barberi et al.*, 1972; *Varet*, 1975; *Varet and Gasse*, 1978; *Hayward and Ebinger*, 1996; *Manighetti et al.*, 2001; *Lahitte et al.*, 2003; *Audin et al.*, 2004]. The rifting episode commenced in September 2005 with a massive dike injection (hereafter called "megadike") that involved opening of the plate boundary, in less than two weeks, of an average 5 m over a length of ~65 km and a depth ranging from ~1–2 km to 10 km. Dike-induced slip on faults in excess of 3 m was reported in some places (Figures 1b and S1a in the auxiliary material and Table 1) [*Wright et al.*, 2006; *Yirgu et al.*, 2006; *Ayele et al.*, 2007; *Rowland et al.*, 2007; *Grandin et al.*, 2009; *Ayele et al.*, 2009].[1] The width of the region where surface breaks were reported in 2005 is less than 5 km [*Grandin et al.*, 2009], and the width of the rift system deduced from analysis of digital elevation data is less than 10 km (Figure 1b) [*Rowland et al.*, 2007].

[9] Seismicity and continuous deformation were detected along the rift in the months following emplacement of the megadike, suggesting ongoing magma movement within the newly intruded dike [*Ebinger et al.*, 2008; *Grandin et al.*, 2010]. From June 2006 to June 2009, a series of twelve smaller dikes (~0.04–0.2 km^3 [this study]) were emplaced in the southern part of the segment that had ruptured in 2005 (Figure 1b and Figures S2a to S13a) [*Hamling et al.*, 2009]. Seismic and geodetic evidences suggest that these post-2005 dikes have their source in a deep-seated magma reservoir lying at the center of the segment, the "Wal'is" magma reservoir (Figures 1b) [*Keir et al.*, 2009; *Grandin et al.*, 2010]. This resembles activity along other rifts, such as the nearby Asal rift in Afar [e.g., *de Chabalier and Avouac*, 1994; *Doubre et al.*, 2007], the Northern Volcanic Zone of Iceland [e.g., *Sæmundsson*, 1979; *Björnsson*, 1985], and segments of the mid-ocean ridge system [e.g., *Lin et al.*, 1990; *Dziak et al.*, 2004]. Transient deformation was observed above the inferred central magma reservoir in the time intervals sepa-

[1] Auxiliary materials are available in the HTML. doi:10.1029/2009JB000815.

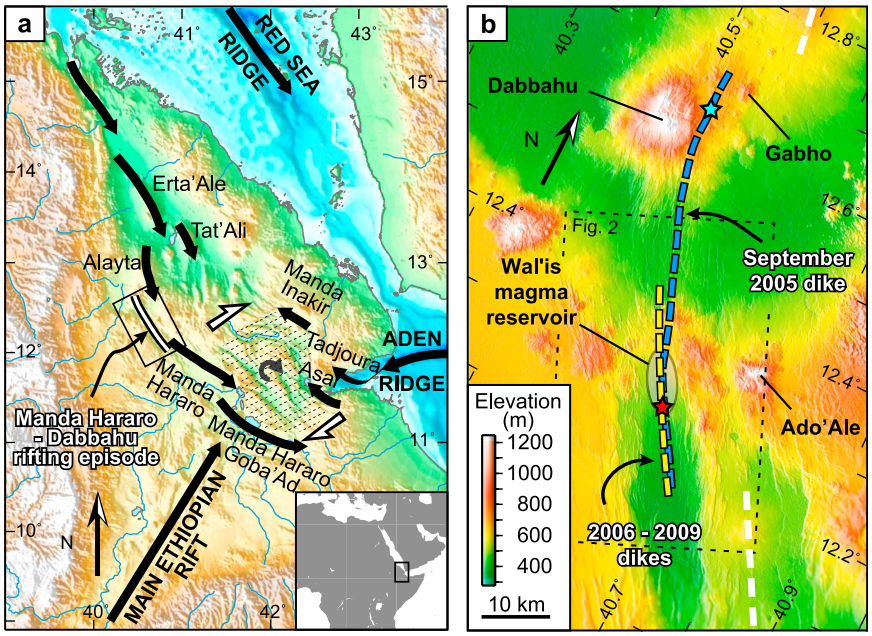

Figure 1. (a) Map of the Afar region. Major rift systems and their propagation direction during Plio-Quaternary are shown with arrows [after *Manighetti et al.*, 2001]. Dashed area in central Afar is affected by block rotations. (b) Digital elevation model (DEM) of the Manda Hararo–Dabbahu rift. Blue and yellow dashed lines indicate the location of dike intrusions that occurred in 2005 and 2006–2009, respectively. Neighboring rift systems of Alayta (to the north) and southern Manda Hararo (to the south) are shown with white dashed lines. Stars indicate the location of eruptions (cyan, silicic; red, basaltic).

rating discrete dike injections, and may be caused by replenishment of the central reservoir [*Grandin et al.*, 2010]. This central reservoir is also likely to have fed the bulk of the September 2005 megadike, except in the northern part of the rift, near to the Dabbahu volcano, where local sources of magma may have contributed to dike inflation [*Grandin et al.*, 2009; *Ayele et al.*, 2009]. Interpretation of the explosive silicic eruption of Da'Ure on 26 September 2005 is debated. The relationship and possible interaction between preexisting magma chambers below Dabbahu on the one hand, and a hot basaltic dike originating from the midsegment magma source on the other, is not well understood due to a lack of data to constrain the sequence of events that took place in September 2005 [*Yirgu et al.*, 2006; *Ayele et al.*, 2007, 2009].

3. Data and Methods

3.1. InSAR Data

[10] For the megadike of September 2005, two pairs of SAR images acquired by Envisat satellite with comple-

Table 1. Dates of the Rifting Events of the Manda Hararo–Dabbahu Rifting Episode[a]

Event	Date	Source	V (km^3)	S (km^2)	X (km)	Z (km)	$\Delta\epsilon$ ($\times 10^{-5}$)	$\Delta\sigma$ (bars)
d0	24 Sep 2005	Seismicity (1,2)	1.822	388.9	-11.0	5.0	23.8	71
d0a	24 Sep 2005		0.777	135.7	-11.0	5.0	49.2	147
d0b	24 Sep 2005		0.417	124.1	3.0	3.5	30.2	91
d1	17 Jun 2006	Seismicity (3), GPS (4)	0.129	118.9	-5.0	3.5	9.9	30
d2	25 Jul 2006	Seismicity (3), GPS (4)	0.048	62.2	1.0	1.5	9.9	30
d3	10 Sep 2006	Seismicity (4), GPS (4)	0.053	98.4	5.0	5.0	5.4	16
d4	7 Dec 2006	GPS (4)	0.044	49.9	-3.0	1.5	12.4	37
d5	14 Jan 2007	GPS (4)	0.037	72.5	5.0	2.5	6.1	18
d6	12 Aug 2007	Modis hot spot (5)	0.055	49.7	1.0	1.5	15.8	48
d7	12 Nov 2007	GPS (4)	0.186	242.9	13.0	4.2	4.9	15
d7a	12 Nov 2007		0.109	108.6	9.0	4.2	9.6	29
d7b	12 Nov 2007		0.077	134.3	23.0	7.0	5.0	15
d8	31 Mar 2008	Seismicity (6)	0.099	161.1	13.0	7.0	4.9	15
d9	9 Jul 2008	Seismicity (7)	0.047	74.2	11.0	0.2	7.3	22
d10	17 Oct 2008	Seismicity (7)	0.198	140.0	-11.0	3.5	12.0	36
d11	11 Feb 2009	Seismicity (7)	0.073	83.5	-5.0	2.5	9.6	29
d12	28 Jun 2009	Modis hot spot (5)	0.044	46.6	1.0	1.5	13.7	41

[a]Source of information that allowed constraint of these dates: 1, *Ayele et al.* [2009]; 2, *Wright et al.* [2006]; 3, *Keir et al.*; 4, *Hamling et al.* [2009]; 5, *Wright et al.* [2004]; 6, *Belachew et al.* [2009]; 7, E. Jacques (personal communication, 2010)). V is dike volume, calculated as the product of average dike opening $\tilde{D}$ and dike surface area S. X and Z givecoordinates of the locus of peak opening deduced from inversion of InSAR data (see Figure 4). Average normal stress changes $\Delta\sigma$ are deduced from displacement-to-length ratios $\Delta\epsilon$ (equation (B1)) multiplied by a Young's modulus of $E = 3 \times 10^{10}$ Pa (see Appendix B).

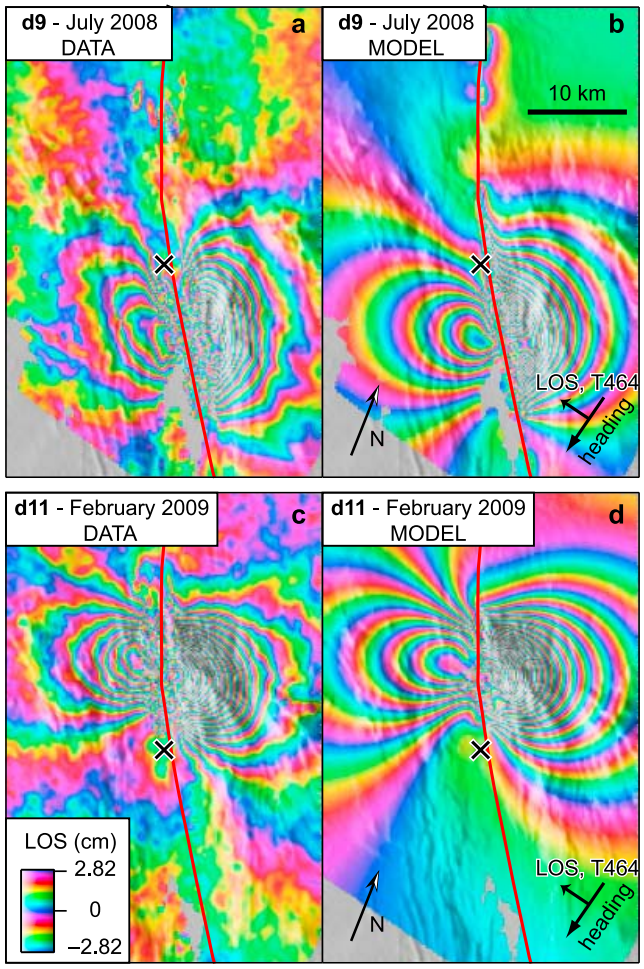

Figure 2. Example of InSAR data and inversion result for dikes (top) d9 (July 2008) and (bottom) d11 (February 2009). (a and c) Line-of-sight (LOS) displacement field on track 464 (descending). Look angle is ~40° with respect to the vertical, and its direction projected on the horizontal plane is indicated by the arrow perpendicular to satellite heading. Increasingly negative range-change (yellow-green-blue-red) corresponds to increasing distance between the satellite and the ground. (b and d) LOS displacement deduced from forward modeling of inversion solution. Location of image is indicated by the dashed rectangle in Figure 1b. Black cross shows the location of the central magma reservoir that fed the dikes. Red line shows the vertical surface along which all dikes occurred.

mentary look directions bracket the date of emplacement of the main dike [*Wright et al.*, 2006; *Ayele et al.*, 2007] (Table S1 in the auxiliary material). Subpixel correlations of these SAR images, as well as subpixel correlations of a set of three pairs of SPOT images, are also available for this event, and the complete geodetic data set for the September 2005 megadike was inverted by *Grandin et al.* [2009].

[11] Since September 2005, systematic SAR acquisitions were performed by Envisat on four different tracks. A total of 12 discrete events of intense surface deformation are identified from June 2006 to June 2009 (Table 1). We processed a series of interferograms that capture each of these events (see Appendix A for details on the InSAR processing). Figure 2 shows two examples of InSAR data imaging the events of July 2008 and February 2009. The InSAR images spanning the 13 events are consistent with deformation caused by intrusion of a series of subvertical planar dikes striking approximately N–S, emplaced at various locations in the Manda Hararo rift [e.g., *Pollard et al.*, 1983] (see also Figures S1a to S13a, which show ascending and descending InSAR data for each dike). Throughout the paper, these events are numbered in chronological order from 0 to 12, with d0 referring to the September 2005 megadike, and d12 referring to last observed dike of June 2009. Dates of the SAR acquisitions used to infer surface displacements associated with each of these dikes are given in Table S1. For all but one event (d5), both ascending and descending InSAR images are available, allowing us to separate unambiguously vertical and horizontal components of surface displacement. For the September 2005 megadike, we only invert InSAR data, and subpixel correlations are discarded. This permits a uniform treatment of dike opening among the different intrusion events.

[12] As shown in Figure 2, each InSAR image shows a semicircular fringe pattern on the side of the rift closer to the satellite due to displacement of the surface toward the satellite. On the other side of the rift, the ground is both uplifted and displaced horizontally away from the satellite, thus yielding a lower number of fringes, also organized in a semicircular pattern. From the location of the fringes, it can be easily concluded that the dikes are emplaced at different latitudes along the Manda Hararo rift.

[13] A finer analysis of the simple fringe pattern described above provides more information about processes occurring at depth. First, the number and width of InSAR fringes as a function of distance from the dike are variable among the different dikes (Figure 2). This indicates variations in the magnitude of the strain field that can be attributed not only to different amounts of dike opening, but also to different depths of emplacement of the dikes [e.g., *Pollard et al.*, 1983] (see also Figures S1d to S13d). Second, fringes are not perfectly semicircular and, in a few cases, are observed to be more broadly spaced toward one end of the dike than the other (Figures S1a to S13a). This may be interpreted as a variation of the depth of maximum opening along the strike of the dike. These second-order features of the fringe pattern provide important insights into the geometry of the dikes at depth. To interpret these details, we use of a model with variable dike apertures. In section 3.2, we describe the inversion scheme and the model geometry, and in Section 3.3, we present our approach for modeling stress changes using the results of these inversions.

3.2. Method for Computing Dike Opening Distributions From InSAR Data

[14] In this section, we describe how InSAR data are inverted to deduce small-scale features of dikes intruded in the Manda Hararo rift. We assume that surface deformation measured by InSAR is caused by tensile opening of a series of dislocations embedded in a homogeneous, linear elastic, isotropic half-space. This approximation is likely to be valid to the first order, as GPS and seismicity data showed that the dikes which occurred in June and July 2006 were emplaced within a few tens of hours at most [*Keir et al.*, 2009; *Hamling et al.*, 2009]. In the subsurface (less than a few kilometers

depth), normal faults and fissures also contribute to the deformation by accommodating the subsidence of a wedge of crustal material above the dike [e.g., *Pollard et al.*, 1983; *Mastin and Pollard*, 1988]. Modeling such deformations requires a more complicated model to account for anelastic processes occurring at low confining pressure [e.g., *Rubin*, 1992; *Wills and Buck*, 1997; *Gerbault et al.*, 1998], which is beyond the scope of this paper. Furthermore, due to decorrelation of InSAR in this area of intense deformation, we were not always able to measure accurately the subsidence that occurred above the dikes. For simplicity, we chose to exclude the area affected by subsidence from our data set. We estimate that the consequence of this choice is that surface displacements associated with dike opening cannot be distinguished from those due to normal faulting for depths in the range of 0–2 km.

[15] The inversion procedure is similar to that described by *Grandin et al.* [2009]. Stratified tropostatic delays affecting InSAR data are removed empirically before the inversion on the basis of a correlation between phase and elevation away from the deforming region. Downsampling of the interferograms is achieved by averaging InSAR data over areas of increasing surface as a function of increasing distance from the inferred average dike plane, using a quad-tree algorithm [*Grandin et al.*, 2009]. For every dike, the weight of InSAR data acquired on ascending and descending tracks is forced to be the same (for instance, if only one ascending image and two descending images are available, the weight of the ascending image is doubled).

[16] InSAR data are inverted to retrieve the distribution of opening of the dikes at depth, using the elastic formulation of *Okada* [1985]. A preliminary inversion aiming at finding the geometry of the dikes (location, strike, dip), following the method of *Tarantola and Valette* [1982], indicates that, except for the September 2005 megadike, we cannot exclude that all dikes have occurred on a single vertical plane. The only exception is the September 2005 megadike, which, north of 12.3°N, is offset by 1–3 km to the east of the trace of subsequent dikes (Figure 1b). For simplicity, we use a common geometry for all dikes: a vertical curved plane is defined, with a trace at the surface following the average position of dikes deduced from preliminary inversion (red line in Figure 2 shows the projection of the modeled dike at the surface). Deviations from a straight plane are small in the region of repeated intrusions: strike equals N163°E at 12.45°N, N149°E at 12.30°N, and N146°E at 12.15°N. The curved plane is discretized into a series of 2 km long dislocation elements (hereafter called "patches"), with increasing widths at depth [e.g., *Lohman and Simons*, 2005]: 2 patches between 0 and 1 km (width 0.5 km), 3 patches between 1 and 4 km (width 1.0 km), 3 patches between 4 and 10 km (width 2.0 km), 4 patches between 10 and 26 km (width 4.0 km), and 4 patches between 26 and 58 km (width 8.0 km).

[17] For the September 2005 megadike intrusion, deflation of three sill-like pressure sources at depth was also tested. These are Dabbahu (40.47°E; 12.57°N; 6.8 km depth), Gabho (40.53°E; 12.69°N; 4.0 km depth) and Wal'is (40.6131°E; 12.3078°N; 20.0 km depth) [*Wright et al.*, 2006; *Ayele et al.*, 2007; *Grandin et al.*, 2009]. However, including these pressure sources in the inversion does not change significantly the resulting opening distribution of the dikes, while introducing additional uncertainty in the inversion, so we preferred to discard them.

[18] A nonnegative least squares inversion scheme is applied (no closure of the dike is allowed). An offset (one parameter) and a tilt (two parameters) for each InSAR image are inverted simultaneously to the opening distribution to account for errors affecting estimates of orbital parameters of the satellite. Introduction of these three additional parameters does not change significantly the resulting opening distribution, while decreasing substantially the RMS misfit in some cases.

[19] Smoothness of the solution is controlled by forcing the inversion to minimize the second derivative of the spatial distribution of opening. A smoothness parameter controls the severity of this constraint. The optimal choice of this parameter is determined on the basis of a compromise between fit to the data and "roughness" of the solution [e.g., *Jönsson et al.*, 2002]. In addition, in this study, a depth dependence of the smoothness parameter is introduced to produce a gradually smoother distribution of opening as depth increases, independently of the imposed increase of patch size as a function of depth: in order to prevent an oversmoothing of the solution at shallow depth and to account for the decreasing resolution as depth increases, we artificially increase the weight of each finite difference smoothing kernel at depth by multiplying each kernel by a factor proportional to the depth of the central patch that the kernel is supposed to represent. With this smoothing scheme, forcing opening to vanish at the bottom of the grid is unnecessary, as well-resolved dike opening at shallow depth becomes spatially separated from deep sectors of the dike that are less well resolved.

[20] Opening deduced from this method is generally small or negligible (<1 m) at depths greater than 14 km, except in a few instances where regions with significant opening (>2 m) appear on the lower parts of the grid, at depth greater than 30 km. However, we noticed that these isolated regions of opening tend to move if we do not invert for the tilt caused by orbital errors. The regions of opening at great depth are interpreted as artifacts, caused by attempts of the inversion to mimic the long-wavelength fringe patterns that can neither be properly modeled by the elastic deformation induced by a dike intrusion at shallow depth, nor by the chosen parametrization of orbital error mitigation. Conversely, opening regions at shallow depth are robust and stable. Thus, opening below 14 km is not considered realistic, and is clipped after the inversion. In the following, the deepest patches that we keep have their middepth at 12 km depth. We checked that the increase of the misfit caused by discarding deep isolated regions of opening is negligible. Secondary regions of opening are also found at shallower depth, in a scattered manner (see for example Figure S10b). However, these generally correspond to opening values much smaller (<0.4 m) than those found on the main dike body (>1 m). These features are likely to represent inversion artifacts and might reflect the amount of uncertainty in our solution caused by propagation in the inversion of errors affecting InSAR data. Yet, we do not mask these latter artifacts, as they do not influence appreciably our results.

[21] Figure 3 shows the distribution of dike opening as a function of time and location along the rift. Figure 4 shows, for each dike, the distribution of dike opening as a function of depth and location along the rift, with the central magma

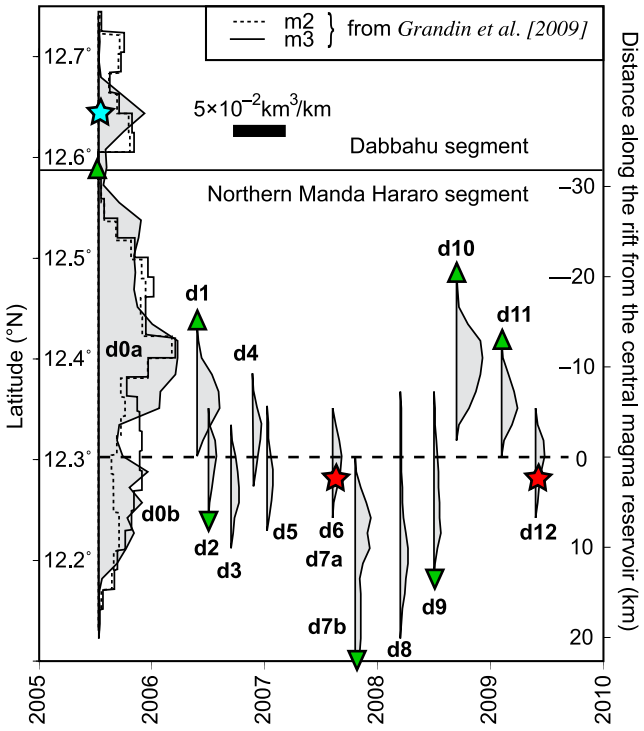

Figure 3. Distribution of dikes as a function of time and latitude deduced from inversion of InSAR data. Thick bar gives the scale for opening distributions. Thickness of the grey curves [this study] indicates dike volume per unit distance along the dike (for instance, dike d10 has an average thickness of ~2 × 10^{-2} km^3/km integrated along its depth and a length of ~10 km, yielding a volume of ~0.2 km^3). For the September 2005 megadike, two end-member solutions for the dike opening distribution of *Grandin et al.* [2009], obtained by a different inversion strategy, are shown for comparison (m2, no central magma reservoir deflation coeval to dike intrusion; m3, magma reservoir deflation at 10 km depth). Distance from the inferred Wal'is magma reservoir at 12.30°N [*Grandin et al.*, 2010] (horizontal dashed line) is shown on the axis of ordinates on the right. Green triangles show the direction of the migration of seismicity during dike injection (from *Ayele et al.* [2009] for megadike d0, *Keir et al.* [2009] for d1 and d2, *Belachew et al.* [2009] for d7, and E. Jacques (personal communication, 2010) for d9, d10, and d11). Stars indicate eruptions (cyan, silicic; red, basaltic).

reservoir representing the origin of the horizontal axis (see also Figures S1b to S13b). These results are discussed in sections 4.1 and 4.2.

3.3. Method for Calculating Normal Stress Change From Opening Distributions

[22] A second part of our analysis is based on the computation of static stress changes induced by successive dike intrusions in order to illuminate the process of dike intrusion. Opening distributions obtained by the method described in section 3.2 are used as an input. In this section, we describe how opening distributions are used to calculate these stress changes.

[23] Slow divergence of the Arabia and Nubia plates is responsible for an accumulation of elastic strain along the plate boundary below the Manda Hararo rift. Dike intrusions act as a means of accommodating this differential motion. Thus, one may consider that dikes fill an opening deficit created by slow elastic stretching of the plate boundary in the interdiking period, which we will call a "tectonic strain deficit." The succession of dike intrusions guarantees that this strain field is heterogeneous in space and that it changes with time.

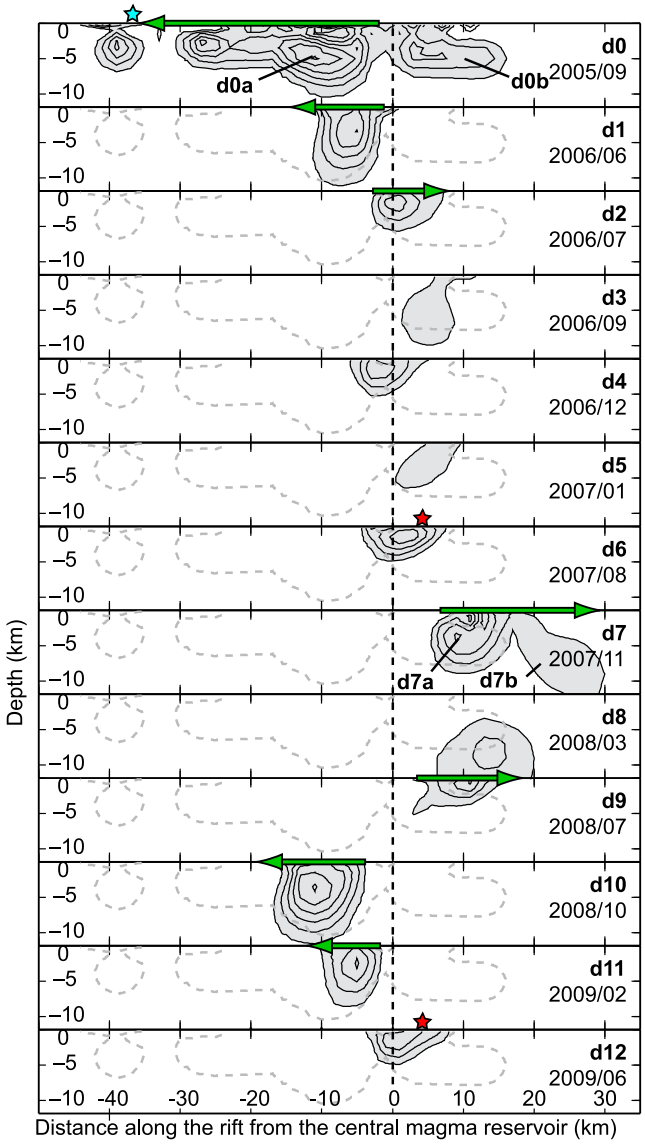

Figure 4. Locations of the 13 dikes intruded between 2005 and 2009 in the Manda Hararo–Dabbahu rift as a function of depth and distance along the rift from the central magma reservoir (dashed vertical line), deduced from inversion of InSAR data. The surface of each dike is indicated by a grey fill. Each contour represents an increment of 2 m opening for the September 2005 megadike (d0) and 0.5 m for other dikes (d1 to d12). The grey dashed contour in the background represents the perimeter of the first megadike (d0) for reference. Stars indicate the location of eruptions. Green arrows above seven dikes indicate the directivity of the dikes, as deduced from migration of seismicity coeval to dike intrusion (see Figure 3 for references).

[24] Implications in terms of stress conditions are the following. In the Afar depression, the occurrence of dike intrusions and the abundance of active normal faults and fissures show that the tectonic context is extensional at the regional scale. The maximum compressive principal stress component σ_1 is vertical, the least compressive principal stress component σ_3 is horizontal, and the intermediate principal stress σ_2, perpendicular to both σ_3 and σ_1, is also horizontal. In such conditions, dikes emplace perpendicular to the direction of σ_3, which is consequently perpendicular to the trend of the Manda Hararo rift (~N155°E) [*Anderson*, 1938].

[25] The magnitudes of principal stresses are more difficult to assess, but dikes can be used as indicators of the shape of the stress tensor [e.g., *Rubin*, 1990]. Here, compressive stresses are defined as positive, and we assume that the relation $\sigma_1 > \sigma_2 > \sigma_3 > 0$ is verified at any time and any depth beyond a few hundred meters [e.g., *Scholz*, 2002]. The tendency for a dike to open in a given region increases as the local magnitude of the driving stress σ_d. This parameter is defined as the difference between magma pressure P, that acts so as to open the dike, and the horizontal stress in the host rock normal to the dike plane σ_3, that tends to counter dike opening [e.g., *Delaney and Pollard*, 1981; *Pollard et al.*, 1983; *Gudmundsson*, 1986; *Pollard and Segall*, 1987; *Rubin and Pollard*, 1987; *Rubin*, 1995]:

$$\sigma_d = P - \sigma_3 \quad (1)$$

According to equation (1), changes in magma pressure will influence the magnitude of driving stress, and "forceful" intrusion of magma driven by its overpressure may occur. However, dikes intruded in environments similar to slow spreading mid-ocean ridges, such as Iceland or Afar, seem to emplace at low magma overpressure [*Rubin*, 1990]. This may imply that the tectonic stress plays the most important role in controlling the magnitude of driving pressure on the plate boundary.

[26] Neglecting for the moment the contribution of magma pressure, much of the information about the propensity for dikes to open in a given region is contained in the local magnitude of σ_3. However, the magnitude of σ_3 is not uniform, nor constant in time, because of stress perturbations caused by dike intrusions [e.g., *Pollard and Segall*, 1987]. These occur in two manners. On the one hand, during dike inflation, a compression occurs perpendicular to the dike, leading to an increase of the magnitude of σ_3 off to the side of the dike [e.g., *Arnott and Foulger*, 1994]. Since dikes tend to open preferentially in areas where the magnitude of σ_3 is lowest (equation (1)), this means that further intrusions off to the side of the dike are less likely to occur shortly after the dike injection [e.g., *Rubin*, 1992]. On the other hand, σ_3 decreases (i.e., stresses become more tensile) beyond the perimeter of the dike off the crack ends, promoting further dike intrusion there [*Pollard and Segall*, 1987].

[27] Conversely, the location and timing of a given dike intrusion are expected to be influenced by the distribution of σ_3, and hence by the history of past dike intrusions. So, we may calculate changes of σ_3 caused by a succession of dike intrusions, and then assess whether a given dike falls in an area of decreased σ_3 as a result of the previous dikes in the sequence, or in an area where σ_3 has been increased, or "consumed", by previous dikes. By analogy with the related problem of earthquake interaction [e.g., *King*, 2007], such an analysis is useful to estimate whether dikes influence each other appreciably, or, to the contrary, whether the perturbation they induce in the ambient stress field is negligible. A similar approach was adopted by *Amelung et al.* [2007] to explain the sequence of earthquakes and dike intrusions at Mauna Loa (Hawaii) from 1983 to 2005.

[28] In the following, we restrict our analysis to the plane of the plate boundary along which dikes were intruded in 2005–2009. We assume that the magnitude of σ_1, which is mostly controlled by the weight of the overlying rock, does not change significantly as a consequence of a dike intrusion, so that only the stress component normal to this plane (σ_3) is relevant for our analysis (yet, the initial distribution of σ_3 is unknown). We also assume that σ_3 does not change direction, and therefore remains normal to the plate boundary at any time between 2005 and 2009. This is likely to be the case, since changes in the strike of the dikes were negligible in this period.

[29] We ignore temporal variations of σ_3 during the intervals between dike intrusions and during dike emplacement itself, and using the opening inversions of section 3.2, we calculate the static normal stress change on the plate boundary induced by each dike intrusion [*Okada*, 1992]. Geometrical and kinematic parameters of the dikes obtained in section 3.2 depend only upon the value of Poisson's ratio ν, but for calculations of stress change, additional knowledge of Young's modulus is required [*Okada*, 1992]. A value of $\nu = 0.25$ is chosen, in agreement with values of $\nu \approx 0.26$ deduced from studies of V_P/V_S ratio in the region close to the Manda Hararo rift [*Berckhemer et al.*, 1975; E. Jacques, personal communication, 2010]. We use a Young's modulus of $E = 3.0 \times 10^{10}$ Pa. This value has been proposed by *Stein et al.* [1991] for modeling crustal deformation due to tectonic loading and magma intrusions in the Asal rift, in eastern Afar, and is consistent with results from mechanical tests of basalt samples in the laboratory at high confining pressure [e.g., *Touloukian*, 1981].

[30] Opening at depth greater than 14 km is clipped for the reasons given in section 3.2. An additional simplification is performed in the stress modeling, whereby patches are collapsed onto a straight plane. The influence of this projection on the resulting normal stress distribution is negligible due to the small deviation from straightness of the curved dike model used in the inversions.

[31] More importantly, stress singularities appear along the edges of each dislocation element. An example of these singularities is shown in Figure 5. They arise from the sharp changes of opening induced by the discretization of the dike plane into a series of dislocations. Similar singularities in the stress field also occur on a larger scale, very close to the crack tip associated with the dike, if dike opening decays fast toward the crack end [*Pollard and Segall*, 1987]. Fortunately, these singularities are limited in size to a small fraction of the crack/dislocation size and may be neglected if we wish to focus on spatial scales of the order of 1–2 km or larger. In order to avoid this local effect, when stress changes are computed from opening distributions, we sample the stress field only at the center of each patch (Figure 5d). The contribution of each opening dislocation is then summed, following the principle of superposition.

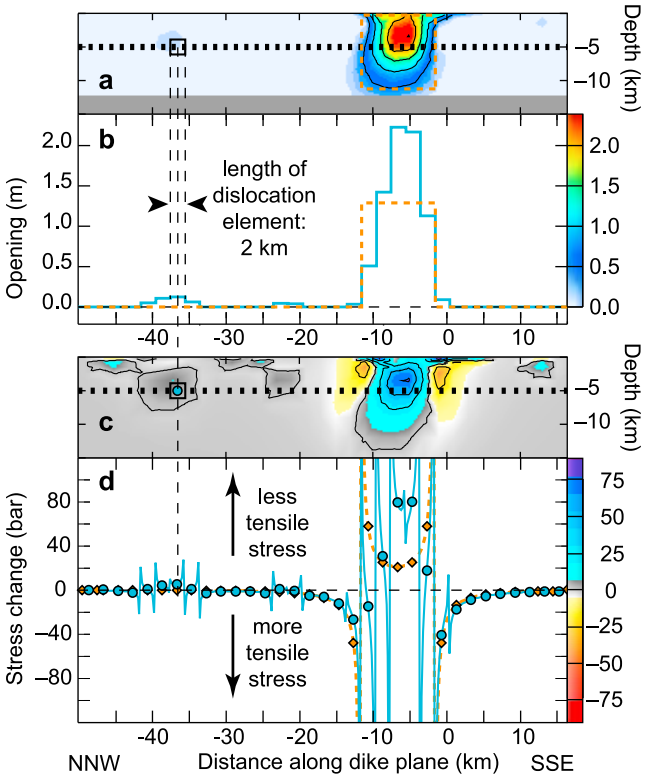

Figure 5. Method for computing normal stress change due to dike injection. Example shows the case of dike d1 (June 2006). (a) Opening distribution on the dike plane deduced from inversion of InSAR data. Orange dashed line shows an alternative, simplified model which consists only of a single element of identical volume. (b) Opening distributions along a profile at 5 km depth (dashed black line in Figure 5a). Blue line shows opening distribution for d1. Orange dashed line shows opening distribution for a single element of identical volume with constant opening (same as in Figure 5a). (c) Distribution of normal stress change (blue, decrease of tensile stress; yellow, increase of tensile stress). (d) Normal stress change along the horizontal profile. Blue line corresponds to a continuous sampling of normal stress change given the opening distribution indicated in blue in Figure 5b. Stress change distribution is rough in this case due to the discontinuities in the opening distribution. Blue dots in Figure 5d show the normal stress distribution sampled at the center of each dislocation element. This coarser sampling is adapted to the grid size and has been used to construct smoothed normal stress change distributions, as shown in Figure 5c. For comparison, orange lines and diamonds correspond to the stress changes deduced for a single dislocation element of identical volume indicated in Figures 5a and 5b.

[32] Opening distributions deduced from InSAR are used here as an input to infer static normal stress change on the plate boundary. As a consequence, the final distribution of stress change on the dike plane relies on the assumption of a regularity of the opening distribution, which is implicitly imposed in the inversions by the smoothing constraints (section 3.2). Smoother or rougher opening distributions in Figure 4 may equally fit surface displacement data, while producing significantly different values of the static stress change: for instance, "sharper" peaks of opening at depth, or overly smeared asperities, would induce higher or lower maximum stress changes, respectively. Therefore, the local value of the normal stress change on the dike plane should be regarded with caution. However, to the first order, the spatial distribution of normal stress change, and the relative location of the regions of stress increase or decrease, constitute a reliable result of our modeling.

[33] Distributions of normal stress change obtained by this method for the 13 dikes of Manda Hararo–Dabbahu rifting episode are shown on the right side of Figure 6 (see also Figures S1c to S13c for normal stress change distributions associated with each dike). These results are discussed in sections 4.3, 4.4, and 4.5.

4. Results and Interpretations

4.1. Spatial and Temporal Pattern of Diking

[34] The dike intrusions of 2005–2009 occurred at different dates and locations along the Manda Hararo–Dabbahu rift, and show a variety of geometrical and kinematic features. In this section, we propose a first interpretation of the sequence of rifting using only space-time arrangement of the dikes (Figures 3 and 4 and Table 1). Here, we rely on InSAR data only to constrain the relative locations of the dikes.

[35] The September 2005 megadike is segmented in three parts [*Grandin et al.*, 2009]: the Dabbahu segment at its northern end and two segments along the northern Manda Hararo rift (Figures 1b and 3). These two latter subdikes (d0a and d0b) are separated by a local minimum of opening at 12.3°N, close to the inferred Wal'is central magma reservoir [*Grandin et al.*, 2009] (Figure 4). Opening north of 12.6°N might reflect an interaction between the northward propagating dike originating from Wal'is, and preexisting magma reservoirs beneath Dabbahu volcano [*Grandin et al.*, 2009; *Ayele et al.*, 2009]. However, this phenomenon is poorly understood, and is not discussed further.

[36] During the 9 months following intrusion of the September 2005 megadike, decelerating inflation of a dike-like pressure source between 4 km and 10 km depth is inferred from InSAR data at the latitude of Wal'is magma reservoir (dashed line in Figure 3) [*Grandin et al.*, 2010]. However, no discrete dike intrusion occurred during that period.

[37] The diking event of June 2006 then inaugurated a sequence of five dike intrusions (d1 to d5) between June 2006 and January 2007, with a recurrence intervals of 1 to 2 months (Figure 3). After a quiescence interval of 7 months, diking resumed in August 2007 (d6), and culminated in an axial eruption on 13 August 2007 [*Yirgu et al.*, 2007; *Ferguson et al.*, 2010]. Dikes d1 to d6 were emplaced within 10 km of the Wal'is magma reservoir (Figure 4).

[38] Following the eruption of August 2007, dike intrusions occurred until June 2009 with a longer recurrence time of 3 to 4 months (Figure 3). The three dikes of November 2007, March and July 2008 (d7 to d9) were emplaced more than 10 km south of Wal'is reservoir, whereas the two following events of October 2008 and February 2009 (d10 to d11) occurred north of Wal'is reservoir (Figures 3 and 4). The last observed dike (d12) was accompanied by an axial

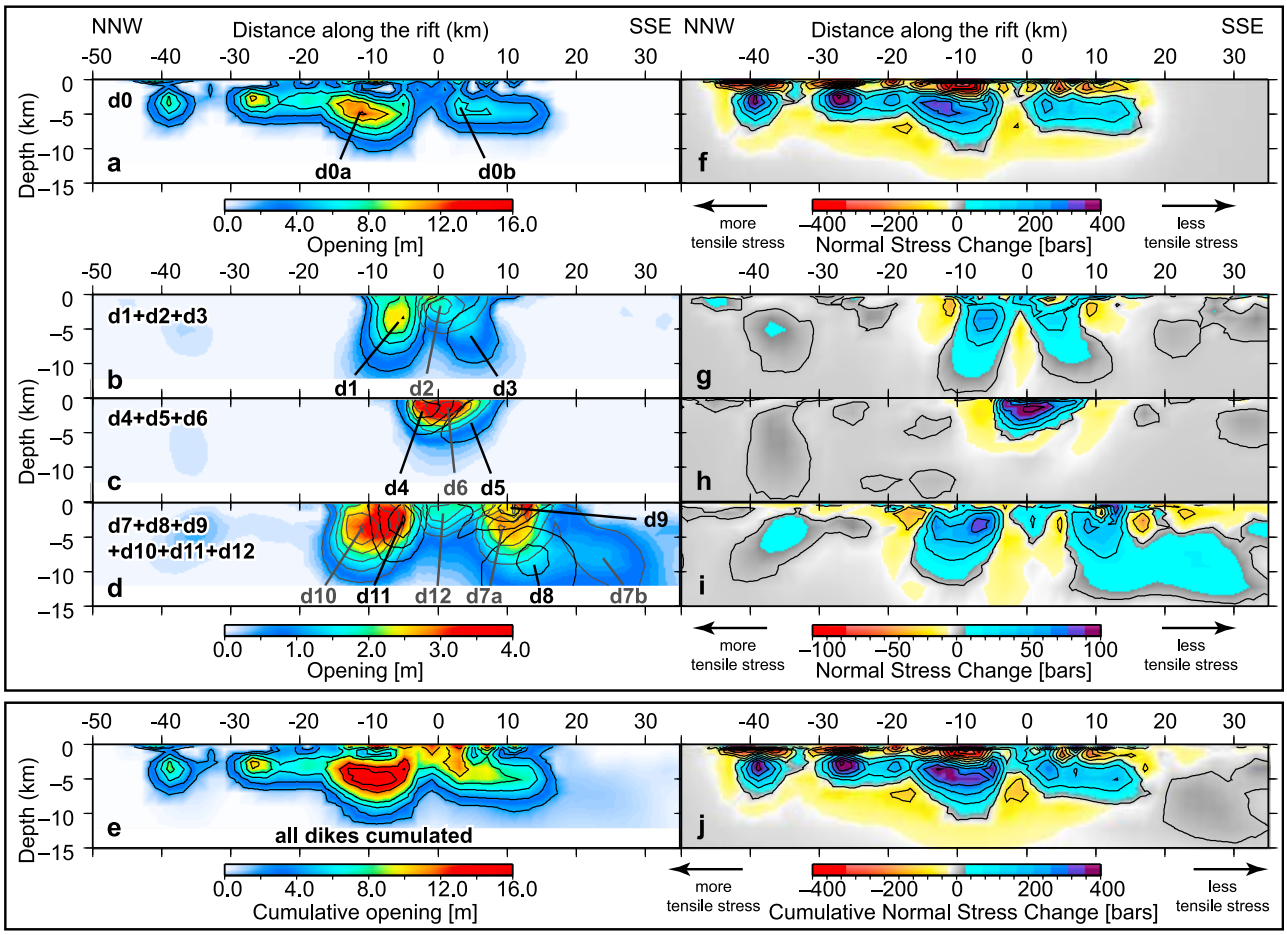

Figure 6. Color images show (left) the cumulative opening or (right) stress change after chosen subsequence of dikes. (a and f) For the first megadike of September 2005 (d0). (b-d and g-i) For dike subsequences d1 to d3 (Figure 6b), d4 to d6 (Figure 6c) and d7 to d12 (Figure 6d). (e and j) The cumulative opening, and corresponding stress change, after the last observed dike d12. For opening distributions, as in Figure 4, contours represent an increment of 2 m opening for the September 2005 megadike (Figures 6a and 6e) and 0.5 m for other dikes (Figures 6b, 6c, and 6d). Distributions of cumulative stress change are contoured accordingly every 100 bars (Figures 6f and 6j) or 25 bars (Figures 6g, 6h, and 6i). Stress change is computed with respect to an unknown initial stress. Note that normal stress change is negative where tensile stress has increased (red-yellow regions). A Young's modulus of $E = 3.0 \times 10^{10}$ Pa was used for calculations of stress change. Distance along the rift is measured with respect to Wal'is central magma reservoir. For a detailed view of each dike intrusion separately (data, model, opening distribution, stress change), see Figures S1 to S13 in the auxiliary material.

eruption on 28 June 2009 (G. Yirgu et al., Afar field trip preliminary report, June 2009, available at http://www.see.leeds.ac.uk/afar/afar_text/Karbahi2_Field_report.pdf, in Afar Consortium communications). This second eruption occurred at the same location as the previous eruption associated with diked 6, and was slightly larger in magnitude and duration than the first eruption [*Ferguson et al.*, 2010] (Figure 4).

[39] Overall, three subsequences of dike intrusions are identified on the basis of the organization of diking as a function of distance from the Wal'is magma reservoir (Figures 3 and 4): (1) proximal dike intrusions, d1 to d6; (2) southerly dike intrusions, d7 to d9; and (3) northerly dike intrusions, d10 to d11. During the two latter subsequences, and possibly also during the first one, dikes seem to have been emplaced at progressively more proximal locations with respect to Wal'is central magma reservoir. An additional observation is that the two basaltic eruptions coeval to dike intrusions d6 and d12, at the end of subsequences 1 and 3, were observed near this inferred magma reservoir. Similar features of spatial and temporal arrangement of dike intrusions were observed during the 1975–1984 rifting episode of Krafla (Iceland) [*Björnsson*, 1985; *Einarsson*, 1991; *Buck et al.*, 2006]. This may suggest that most, if not all, dikes that occurred during the Manda Hararo–Dabbahu rifting episode have their source in a single magma reservoir near the center of the rift. This is in agreement with the observed directivity of earthquake migration during emplacement of at least six dikes (Figures 3 and 4) [*Keir et al.*, 2009; E. Jacques, manuscript in preparation, 2010]. Furthermore, for the most distal dike intrusions (d7 to the south, and d10 to the north),

we notice that a few InSAR fringes could not be modeled by our dike model. These residual fringes occur at the location of the inferred magma reservoir, and the bull's eye shape of the fringes (see residues in Figures S8 and S11) is characteristic of deflation of a magma chamber at depth, providing evidence for a counterpart to dike inflation. The time between successive dike injections is likely controlled by the rate of repressurization of this reservoir after it has experienced the abrupt pressure drop coeval to dike escape [*Grandin et al.*, 2010].

4.2. Opening Distributions

[40] The opening distributions deduced from inversion of InSAR data (section 3.2) are model and related assumptions dependent and should be treated with caution, especially when interpreting small-scale features. For instance, the trade-off between magnitude of opening and depth of opening introduces significant uncertainty in the inversion, which is difficult to quantify. However, because the InSAR data set has been processed using a uniform inversion method, the various biases affecting the inversion results are expected to be the same for all dikes, whereas the differences between the dikes are likely to be well constrained. Keeping these limitations in mind, we compare the locations and opening distributions of the dikes as a function of time (Figures 4 and 6a–6e and Table 1).

[41] Maximum opening of ~12 m occurs in the central part of the September 2005 megadike, at a depth of ~5 km (subdike d0a). About 10 km further south, another local opening maximum of ~7 m occurs (subdike d0b) (Figure 4). These two subdikes represent total volumes of magma of 0.8 and 0.4 km^3, respectively. Subsequent dikes intruded from 2006 to 2009 have volumes smaller than that of the September 2005 megadike by one order of magnitude (0.04–0.2 km^3), and generally exhibit simple convex opening distributions, with a maximum opening ranging from 0.8 m to 3.5 m, and a peak opening occurring between 0.5 km and 7 km depth. The geometry of these dikes resembles the blade-like dikes of *Rubin and Pollard* [1987]. The November 2007 event may consist of two distinct subdikes (named d7a and d7b) (Figure 4).

[42] The deformation pattern imaged by InSAR suggests that groups of dikes may exist that produce a very similar shape of the deformation field at the surface. Within the framework of the theory of linear elasticity, this observation is interpreted as being due to an almost identical geometry of the intrusion (depth, latitude, rupture area), but different magnitude of the inflation (Figures 4 and 6a–6e). The first group consists of dikes d6 and d12, and possibly d2 (see Figures S3a, S7a and S13a). These dikes were emplaced at shallow depth, above Wal'is magma reservoir, and the two most recent dikes d6 and d12 were both accompanied by lava extrusion (Figure 4). The second group is composed of dikes d1 and d11, which intruded along a 10 km long segment north of Wal'is magma reservoir (see Figures 4 and S2a and S12a). A third group includes dikes d0a and d10, as the peaks of maximum opening of these two dikes are located at nearly the same depth and latitude (Figures 6e, S1a, and S11a). This may suggest that sequences of dikes d0a-d1-d2 on one hand, and d10-d11-d12 on the other hand, follow the same pattern.

[43] Despite the possible existence of a few multiple events, most dikes in the 2006–2009 sequence seem to occupy different depths and/or latitudes along Manda Hararo rift. This may suggest that the tectonic strain deficit accumulated since the previous rifting episode is progressively filled by successive dike intrusions on the plate boundary until differential stress is completely relieved [e.g., *Björnsson*, 1985]. For instance, most dikes in 2006 and 2007 (e.g., d2, d4, d5, d6, d7b, d8,d9, d12) seem to fill deficits of opening associated with the September 2005 megadike (see Figures 4 and 6a) [see also *Hamling et al.*, 2009]. More surprisingly, a few other dikes, including the most voluminous ones (e.g., d1, d10 and d11, but also d3, and d7a) appear to have been emplaced at locations that had previously experienced a large amount of opening in 2005 (Figure 4). This feature will be addressed in more detail in section 4.5.

[44] Another key observation is that depth of dike opening is observed to increase at greater distance from the central magma reservoir (Figures 4 and 7a). This may reflect the thickening of the elastic-brittle crust toward segment ends, allowing for the possibility of a higher resistance of the crust, and less frequent, thicker dike intrusions [*Rubin*, 1995]. This is compatible with the presence of a mantle upwelling at the center of the segment where magma generation and/or melt ascent in the lithosphere are focused, such as at mid-ocean ridges [*Shaw and Lin*, 1996; *Dunn et al.*, 2005] or the Asal rift, in eastern Afar [*Doubre et al.*, 2007]. Unfortunately, no geophysical data are currently available to constrain along-axis variations of the thickness of the brittle-elastic lithosphere in the Manda Hararo rift.

[45] Finally, the distribution of dike opening as a function of distance from the central magma reservoir suggests that more voluminous dikes tend to travel further (Figure 7b). This is the case of d7 and d8 to the south, and d1 and d10 to the north. Although the problem of identifying the magma pathway for such distant dikes is not resolved, their larger volume (with respect to more proximal dikes, like d2, d3, d4, d5, d6, d12) may indicate that driving stress is higher toward segment ends to the northern and southern ends of Manda Hararo rift. Since magma pressure in the dike is likely to decrease as the dike is emplaced at increasingly large distance from the source reservoir, a high driving stress toward segment ends may be due to a larger magnitude of tensile stress on the plate boundary there. A more complex modeling approach, that would include thermomechanics of dike intrusions and magma storage, is required to investigate this point.

4.3. Normal Stress Changes off to the Side of the Dikes

[46] In this section, we describe first-order features of the variations of the stress field along the dike bodies off to their sides, and we attempt to draw an analogy between dikes and earthquakes within the framework of linear elastic fracture mechanics (Figures 6f–6j and 7c and Table 1).

[47] Prior to the onset of a rifting episode, the brittle crust is stretched, and opening of a dike relieves a fraction of the accumulated tension. The initial tensile stress is thus locally lowered by a dike intrusion (section 3.3). We recall that increases of σ_3 correspond to more compressive, or less tensile stress conditions. The corresponding changes in driving stress (equation (1)) imply that dike intrusions are

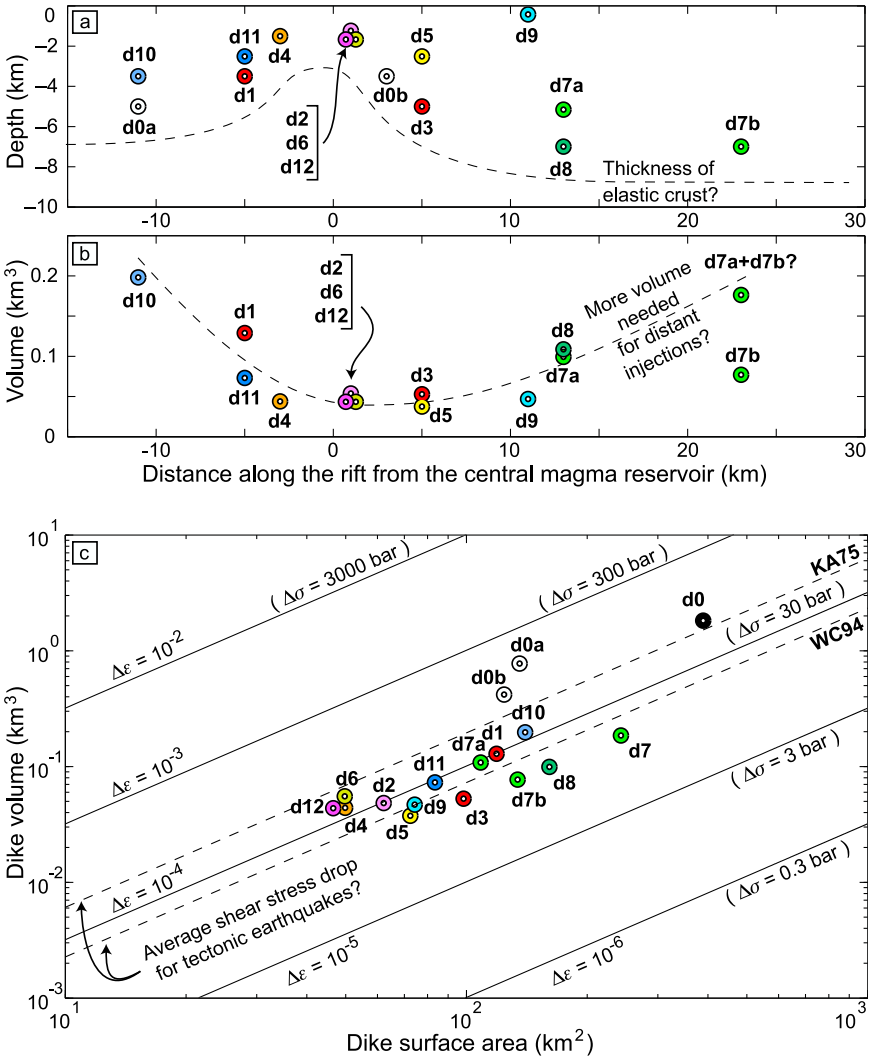

Figure 7. (a) Depth of the dikes as a function of their location along the rift (the dots indicate the location of peak opening for each dike). Dikes of September 2005 (d0) and November 2007 (d7) have been split in two subdikes (see text for discussion).(b) Volume of the dikes as a function of their location along the rift (the dots indicate the location of peak opening for each dike). Megadike d0, with a total volume of 1.2 km^3, is not shown, for clarity. In Figures 7a and 7b, the origin of the horizontal axis is taken at the location of Wal'is magma reservoir at 12.30°N (Figure 3). (c) Dike volume versus surface area (grey fill in Figure 4). Solid lines represent the trend for a constant displacement-to-length ratio $\Delta\epsilon$. Between parentheses, equivalent stress changes $\Delta\sigma$ using a modulus of 3×10^{10} Pa are indicated. Dashed line shows trend for a shear stress drop of 21 and 60 bars relevant for tectonic earthquakes, deduced from scaling relationships by *Wells and Coppersmith* [1994] (WC94) and *Kanamori and Anderson* [1975] (KA75), respectively.

promoted in areas of decreased σ_3, whereas dikes are less likely to open in regions where σ_3 has increased.

[48] The normal stress σ_3 locally increased by more than ~300 bars in September 2005 in the area of maximum opening of the megadike (d0a), and by only ~150 bars in the southern part of the dike, where magnitude of opening was lower (d0b) (Figure 6f). Later dikes induced a local increase of σ_3 by ~25–100 bars on the dike plane in their respective areas of maximum opening (Figures 6g–6i). Locally large positive or negative values of stress change also appear at depths shallower than 1–2 km because opening distribution is rough in our inversions in this depth range (Figure 6j). Actually, such high tensions/compressions are likely accommodated by slip on faults in the subsurface and the distributed opening of fractures. This effect, which is strongest after the September 2005 megadike, is therefore an artifact caused by our choice to ignore faults in the modeling (section 3.2). We do not discuss this point further.

[49] As seen in section 4.2, opening distributions associated with dike intrusions in the Manda Hararo rift in 2005–2009 suggest that dikes may be described, to the first order, as cracks in an elastic body. Our elastic inversions allow to calculate the stress changes associated with these dikes, using directly the surface and average opening of the dikes.

Stress changes obtained in this manner may be compared with the static shear "stress drops" for tectonic earthquakes [e.g., *Scholz*, 2002] (see Appendix B for more details on the calculations). We define the decrease in tensile stress averaged on the surface of the dike coeval to intrusion as the "average normal stress change" (Figure 7c and Table 1). The average normal stress changes associated with dikes in 2006–2009 in the Manda Hararo rift are in the range of 15–50 bars, and up to 70 bars for the September 2005 megadike (perhaps reaching 150 bars on subdike d0a). These values are comparable with the static shear stress drops of 20–60 bars caused by earthquakes releasing similar amount of strain energy [e.g., *Kanamori and Anderson*, 1975; *Wells and Coppersmith*, 1994; *Allmann and Shearer*, 2009]. The displacement-to-length ratios for dikes in the Manda Hararo rift ($20–50 \times 10^{-5}$) are thus the same as those of earthquakes with similar rupture areas (in the range of 50–150 km^2, corresponding to magnitudes $M \sim 6$). This feature may be typical of dikes intruded at low magma pressure and high differential stress, such as in the volcanic rift zones of Iceland [*Rubin*, 1990]. The low-pressure hypothesis is further supported by absence of inflation of the Wal'is magma chamber prior to the September 2005 megadike intrusion [*Grandin et al.*, 2009]. This observation may be an indicator of the predominant role of tectonic stress in driving dike intrusions in the tectonic context of the Manda Hararo rift.

[50] However, occurrence of multiple events of similar magnitude emplaced in nearly the same region of the plate boundary, but separated by intervals of time much shorter than characteristic time of tectonic stress buildup, is not typical of earthquakes. The cause of this phenomenon likely arises from the limited magma availability at the onset of dike propagation due to the limited size of the source reservoir feeding the dikes, or, in other words, its inability to sustain high magma pressure during dike expansion [*Buck et al.*, 2006; *Rivalta*, 2010]. So, even if dike opening does not involve contact between the dike walls, limited magma availability may be envisioned as the counterpart of some kind of "dynamic friction" in earthquake phenomena, for it limits the amount of differential stress that can be relieved by a single event. The equivalent of a "static friction" may be found in the threshold of driving stress in the neighborhood of the source reservoir that must be reached to nucleate a dike. Unfortunately, the overwhelming importance of fluid mechanics in driving dike intrusion, in contrast to the process of earthquake rupture, prevents us to make further analogies.

4.4. Cumulative Increase of Tension in the Vicinity of the Magma Source

[51] As shown in Figure 5 and discussed in section 4.3, coeval to magmatic intrusion, σ_3 increases off to the side of the dikes, but σ_3 also decreases beyond the perimeter of a dike, thus facilitating future dike opening there. In this section, we focus our analysis on the stress change beyond the surfaces of the dikes, off crack ends (Figures 6f–6j). We recall that this approach is likely affected by several sources of uncertainty and associated errors originating from various origins. For instance, opening distributions deduced from inversion of InSAR data are model and geometry dependent. Furthermore, departure from a purely elastic behavior may distort surface displacement fields, which may bias our inversions. Also, our analysis implicitly neglects the existence of important variations in magma pressure in the source magma reservoir at the beginning of dike intrusions. Finally, transient phenomena that might have occurred shortly after or before dike intrusions would be undetected by the geodetic data presented here. Despite these limitations, the uniform handling of InSAR data presented in this study ensures that a consistent treatment is applied to all dikes, and that the differences between strain fields induced by the different dikes at the surface provide reliable information on the relative locations and volumes of the dikes, which are the two basic informations used in our stress modeling.

[52] After intrusion of the September 2005 megadike, σ_3 decreased by more than 100 bars beneath the local minimum of opening between d0a and d0b, approximately at the latitude of the central magma reservoir (Figure 6f). Subsequent dike intrusions occur above the point of maximum decrease of σ_3 at shallow depth (1–4 km depth), leading to a total cumulative decrease of σ_3 by as much as 150 bars at the end of the sequence of dike intrusions of 2005–2009 (orange region in Figure 6j at 0 km along the rift and 6 km depth). This localized increase of tension emerges because no discrete dike intrusion event has occurred at any time in the center of the rift at a depth greater than 4 km (section 4.2). This is in keeping with information from seismicity migration during dike emplacement, and codiking deflation imaged by geodesy, which show that this location is approximately that of the inferred source of magma for dike injections [*Ayele et al.*, 2009; *Hamling et al.*, 2009]. In addition, this area of increased tension on the plate boundary is precisely the locus of transient events of rift-perpendicular opening in the 4–10 km depth range, occurring in the weeks/months following most dike injections, as revealed by InSAR [*Grandin et al.*, 2010].

[53] We propose that the absence of deep discrete dike injection at the center of the rift may be caused by the presence of a local thinning of the brittle-elastic crust in this area, possibly due to proximity of a midsegment heat source associated with focused magma percolation and ascent (Figures 4 and 7a). The slow opening transients reported by *Grandin et al.* [2010] are not compatible with a simple brittle-elastic rheology there and may be caused by a deformation process leading to gradual relaxation of at least part of the increased tensions caused by dike intrusions. However, the physical mechanism responsible for the delayed response of the lithosphere in this area (continued dike opening at depth, viscoelastic process, interaction with pressurized magmatic fluids, etc.) is poorly understood [see *Grandin et al.*, 2010].

4.5. Interactions Between Dikes

[54] In this section, we follow the evolution of the normal stress σ_3 on the dike plane as a function of time, in order to assess the possibility of static triggering between dikes in the 2005–2009 sequence (Figures 6f–6j and 8). We use an approach similar to that adopted for earthquake sequences, following *Amelung et al.* [2007] (for a review of stress interaction between earthquakes, see also *King* [2007]).

[55] In Figure 8, we have plotted the cumulative change of σ_3 as a function of time, for a series of target locations on the dike plane. These locations are chosen to correspond to loci of peak opening ($D > 0.9D_{max}$) during the successive

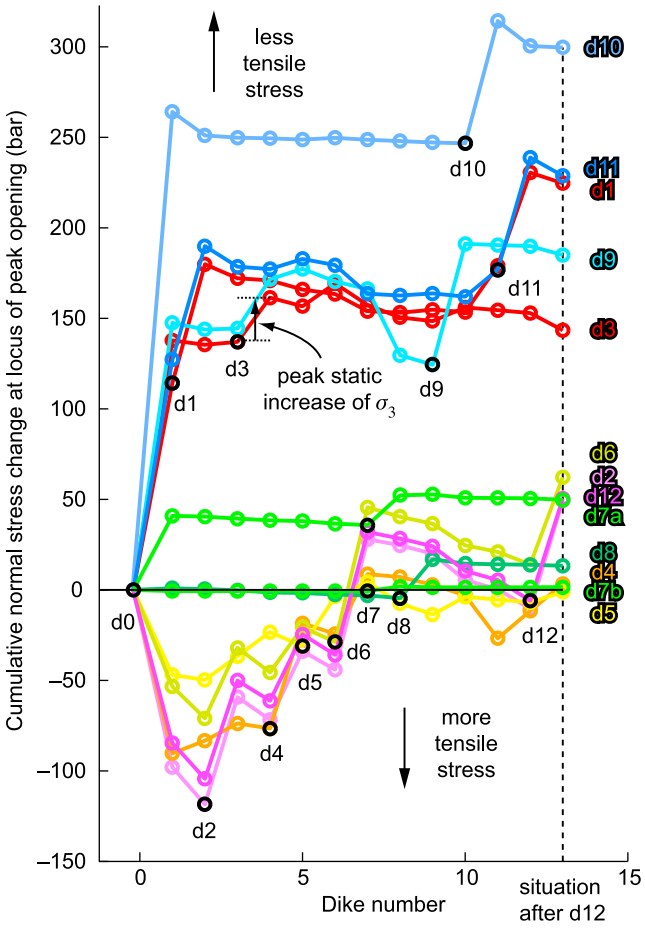

Figure 8. Evolution of the cumulative normal stress change at the location of each dike over the duration of the rifting episode (location is chosen as the locus of peak opening, shown in Figures 4 and 7a). Stress change is computed with respect to an unknown initial stress. Note that normal stress change is chosen negative where tensile stress increases (regions in yellow on the right part of Figure 6). Values on the far right give the stress change after last observed dike d12 (Figure 6j). For each dike, black circle shows the local value of stress prior to intrusion of the dike. For all cases, with the exceptions of dikes d1, d3, d10, and d11, tensile stress increased in the area of emplacement of the upcoming dike as a result of intrusion of the previous dike in the sequence.

dike intrusions (Figure 4). The static stress changes following September 2005 megadike injection are summed, in order to assess whether a given dike lies in an area of increased or decreased σ_3 at the time of dike intrusion, given the succession of previous dike intrusions in the sequence. The stress values prior to September 2005 are unknown, and any change of tensile stress in the 2005–2009 interval caused by far-field tectonic loading, or continuous deformation at depth during that period, is not taken into account.

[56] All dikes north of Wal'is (d1, d10 and d11), and three dikes to the south (d3, d7a and d9), were emplaced in areas where σ_3 had already increased (i.e., where tension has decreased) as a result of intrusion of the September 2005 megadike (Figure 8). This indicates that all the initial (tensile) differential stress was not relieved fully by the first dike injection, possibly because not enough magma was available (section 4.3). However, despite a higher magnitude of σ_3 in 2006–2009 than before September 2005, and hence a lower driving stress (equation (1)), it was still possible for magma to be emplaced into a series of thick dikes in regions already opened by megadike d0 (see dikes d3, d7, and d10 in Figure 4). Three possibilities may explain this observation: (1) magma pressure was higher in 2006–2009 than in 2005, allowing injections to be triggered despite an overall decrease of tension in the brittle crust; (2) rupture of the elastic-brittle crust was made easier in 2006–2009 than in 2005 due to a decreased resistance of host rock in the region of emplacement of the previous dikes; and (3) rupture of the reservoir roof/wall, and escape of magma, was made easier in 2006–2009 than in 2005 due either to a lowered resistance to fracture of the magma reservoir or increased tension around the magma reservoir due to stress transfer induced by nearby injections. Identifying the most likely hypothesis requires knowledge of magma pathway, which is still debated. However, the fact that the three largest events in this population of 2006–2009 dikes (d1, d10 and d11) were in the upper range of dike injections in terms of volume (Figure 7b), and all occurred north of the inferred central magma reservoir (Figure 3), may indicate that tension was highest in that part of the rift in 2006. The greater tension there may have been capable of attracting the most voluminous dikes in the sequence. This may still be the case, and one might expect more injections there in the future.

[57] Figure 8 shows that all other dikes (d2, d4, d5, d6, d8 and d12) emplaced in areas of decreased σ_3 with respect to the value before September 2005. In our modeling, these increased tensions are due to the stress transfer induced by the September 2005 megadike. As successive intrusions occurred in 2006–2009, σ_3 progressively increased, so that after the last observed intrusion of June 2009 (d12), normal stress computed at the loci of maximum opening of these dikes had nearly returned to the initial level before September 2005. Consequently, the cumulative opening of these dikes appears to have just compensated for the decrease of σ_3 induced by the September 2005 megadike alone (Figure 8). This may indicate that these dikes were triggered primarily by megadike d0, and need not correspond to the relief of differential stress accumulated before September 2005.

[58] These smaller dikes occurred at shallow depth, in most cases near to the magma source (Figure 4). Furthermore, little opening occurred in this region in September 2005 (Figure 4). These observations suggest that differential stress was relatively low in this area both before and after September 2005. In addition, two dikes (d6 and d12) were associated with axial basaltic eruptions approximately above the central magma reservoir (Figure 7). This suggests that magma excess pressure and/or buoyancy dominates over tectonic stress in the vicinity of the magma source, possibly as a result of a lower resistance of the thinned lithosphere there [e.g., *Gudmundsson*, 1986]. We could expect that dike intrusions that may occur in the following months (if any) in this area will be both smaller, and associated with more copious effusive activity, as remaining tensile stress may be low in the

vicinity of the central magma reservoir [e.g., *Buck et al.*, 2006].

[59] The case of dike d9 is interesting in its own right: although it occurred at shallow depth, this dike was emplaced in an area of decreased tension with respect to before dike d0 (Figure 8), so that its interpretation is problematic. However, this dike induced an increase of σ_3 slightly greater than the decrease of σ_3 transferred by dike d7 alone. We also notice that the magnitude of the decrease of σ_3 at d9 induced by d7 is the highest of all decreases of σ_3 calculated throughout the rifting episode for any other pair of dikes between 2006 and 2009 (Figure 8). This is due to the surprising complementarity of opening distributions of dikes d7a and d9, the latter dike filling a local minimum of opening of the first dike (Figure 4). Thus, given the uncertainty on the initial stress conditions, dike d9 may also belong to a category of dikes triggered by stress change caused by the previous dike(s) in the sequence. In this view, taken as a whole, the sequenced 7b-d8-d9, which occurred ahead, above and below the limits of dike d0b, respectively (Figure 4), may represent a southward propagation of the rupture initiated in September 2005. Repeated inflation during previous dike intrusions d0b, d3 and, finally, d7a may have provided the conditions that led to its eventual growth. In addition, we may speculate that the magma emplaced in dikes d8-d9 flowed through the body of dike d7a to reach the crack tip region, as dike d7a, with a maximum thickness of 2 m, may have remained open for several months (the solidification time scales with the square of dike thickness, and a dike that is several meters thick may require years to freeze by conduction [*Turcotte and Shubert*, 1982; *Carslaw and Jaeger*, 1986]). However, more data are required to support this hypothesis.

5. Conclusions

[60] The 13 rifting events that occurred from September 2005 to June 2009, in the Manda Hararo rift in Afar (Ethiopia), as part of an ongoing rifting episode, provide an unprecedented opportunity to illuminate the process of dike intrusion at a divergent plate boundary. Using InSAR data, we invert for dike opening as a function of depth and location along the rift. Resulting opening distributions are then used to compute distribution of static normal stress change on the plate boundary as a function of time. Our models rely on a series of hypotheses. The first is that the lithosphere behaves in an elastic manner on the timescale of dike emplacement (a few tens of hours). Also, we assume that dikes preferentially emplace in sectors of the plate boundary where tensions are highest. Finally, we suppose that dikes are fed by a midsegment magma reservoir located below the rift. Keeping these assumptions in mind, we interpret the space-time evolution of diking during the current rifting episode using a variety of approaches.

[61] Inversion of InSAR data shows that dikes were emplaced between 0 and 12 km depth, with thicknesses of 0.8–3.5 m (up to 12 m peak opening for the September 2005 megadike), lengths of 10–15 km (65 km in September 2005), and volumes of 0.04–0.2 km^3 (probably > 1 km^3 in September 2005). Dikes are intruded north, south or above of the inferred magma reservoir located in the middle of the segment ("Wal'is" magma reservoir).

[62] Cumulative opening distributions of the dikes suggest that the thickness of the lithosphere intruded by dikes is least at the latitude of this midsegment magma reservoir (~4–6 km), and is thicker toward segment ends (~10–12 km). Near the magma reservoir, no deep discrete dike intrusion is observed, but slow deformation has been reported in the time intervals separating diking events [*Grandin et al.*, 2010]. This is compatible with the presence of a "hot" thermal anomaly caused by focused melt ascent from below the lithosphere, responsible for a shallowing of the brittle-ductile boundary there, in analogy with observations made at slow spreading mid-ocean ridges [e.g., *Lin et al.*, 1990; *Shaw and Lin*, 1996; *Dunn et al.*, 2005].

[63] The average normal stress changes during individual dike intrusions off to the sides of the dike bodies are in the range of 15–50 bars (up to 70–150 bars for the September 2005 megadike), using a "reduced" Young's modulus of $E = 3.0 \times 10^{10}$ Pa. This is comparable with the average static shear stress drop reported for tectonic earthquakes, possibly suggesting that rifting in the tectonic context of the Manda Hararo rift is mostly controlled by tension in the brittle lithosphere as a result of boundary conditions imposed by divergence of tectonic plates. These dikes, similarly to those observed in the Northern Volcanic Zone of Iceland, or at magma-poor slow spreading mid-ocean ridges, seem to be driven primarily by tectonic stress and to intrude at low magma pressure [*Rubin*, 1990].

[64] We identify groups of successive dike intrusions that are clustered in space and time, suggesting that dikes interact, and are not randomly distributed on the dike plane. The observation that the most voluminous dikes in the 2006–2009 sequence (d1, d10 and d11) broke sections of the plate boundary that had been already opened by the September 2005 megadike by as much as ~10 m, suggests that the deficit of opening accumulated since the previous rifting episode ($\sim 10^2$–10^3 years ago) has remained high at that location throughout the duration of the current rifting episode. Other smaller dikes, less distant from their inferred midsegment source (d2, d4, d5, d6 and d12), seem to fill local minima of opening of the initial megadike intrusion of September 2005. Two dikes propagated to the south of the magma reservoir and have been emplaced in regions that had only moderately opened in 2005 (d3 and d7a). They were followed by events that extended the rupture area to the south, beyond the limits of the 2005 megadike (d7b, d8 and d9). These observations suggest that models attempting to explain the succession of dike intrusions during a rifting episode should take into account the possibility that stress transfer may play a role in triggering at least some of the dike intrusions during a rifting episode.

[65] Normal stress modeling also indicates an apparently higher opening deficit north of the Wal'is magma reservoir, compared to the southern part of the rift, both before and after emplacement of the September 2005 megadike. This is not compatible with the driving stress being primarily controlled by the along-rift axial topographic profile [e.g., *Fialko and Rubin*, 1998], as both sections of the rift are characterized by similar elevations. Rather, as suggested by *Buck et al.* [2006], the initial distribution of (tensile) differential stress on the plate boundary, controlled by the history of previous rifting episodes that ruptured partially the plate interface in the past [e.g., *Björnsson*, 1985], and/or the difference in

crustal thickness resulting from a structural or thermal inheritance on geologic timescales [e.g., *Rubin*, 1995], may exert a greater control on the style and succession of rifting events and associated eruptive manifestations.

Appendix A: InSAR Processing

[66] A total of 235 interferograms were computed. InSAR data were processed with ROI$_{PAC}$ software [*Rosen et al.*, 2004]. Envisat state vectors calculated by ESA using DORIS orbits were used to subtract the orbital fringe pattern [*Zandbergen et al.*, 2002]. The topographic contribution to the interferometric phase was subtracted using a 90 m SRTM DEM [*Farr and Kobrick*, 2001]. Unwrapping was performed using a cut-tree algorithm [*Goldstein et al.*, 1988]. Topography-correlated tropospheric delay [e.g., *Beauducel et al.*, 2000; *Hannsen*, 2001] was removed empirically from each InSAR image by determining a linear regression between phase and altitude on surrounding volcanic edifices where deformation is assumed to be absent [see, e.g., *Cavalié et al.*, 2007]. A planar trend is simultaneously subtracted from LOS data in the regions not affected by codiking deformation in order to reduce bias induced by orbital errors.

[67] The periodicity of dike intrusions from June 2006 to June 2009 is sufficient to enable the retrieval of codiking interferograms for most events on both ascending and descending tracks. Furthermore, for each track independently, a pixel-by-pixel time series inversion was performed on InSAR data to deduce LOS displacement between every two successive SAR acquisitions, with a maximum sampling rate of 35 days [e.g., *Berardino et al.*, 2002; *Schmidt and Bürgmann*, 2003]. A total of 42 InSAR measurements are obtained by this technique (Table S1). For 10 dikes out of 12, both ascending and descending LOS deformation data closely bracketing the diking event are available. For the two dikes of December 2006 and January 2007, which are separated by a very short interval in time, sparse SAR data do not allow the events to be easily separated, as the only interferograms from the descending track (464) include the cumulative deformation produced by the two events. A specific procedure was applied for these two dikes. For the January 2007 event, codiking deformation was inverted with data from ascending tracks 28 and 300 only (see section 3.2). Then, synthetic deformation deduced from the solution of the inversion was projected onto LOS vector of track 464, and the resulting synthetic LOS displacement was subtracted from the interferogram of track 464 that images both events. The resulting LOS deformation on track 464 thus includes the deformation produced by the December 2006 event only, plus modeling errors. It was then inverted jointly with InSAR data on tracks 28 and 300 spanning the December 2006 event.

Appendix B: Method for Calculating Average Strain-Stress Changes

B1. Definition of Strain and Stress Changes

[68] Within the framework of linear elastic fracture mechanics, both dikes and earthquakes may be represented as cracks in an elastic body: mode I tensile cracks in the case of dikes, mode II or III shear cracks for earthquakes [*Scholz*, 2002]. The average strain change $\Delta\epsilon$ associated with crack models is defined here as proportional to the ratio between average relative displacement of the cracks faces $\tilde{D}$, and characteristic length scale of the crack L, approximated here by the square root of crack area S:

$$\Delta\epsilon = C\frac{\tilde{D}}{L} \approx \frac{\tilde{D}}{\sqrt{S}} \tag{B1}$$

where C is a constant that depends on the geometry of the crack [e.g., *Eshelby*, 1957; *Aki*, 1972]. For a roughly circular crack, $C \sim 1$ [*Kanamori and Anderson*, 1975]. For simplicity, we assume that $C = 1$, hence the approximate formula in equation (B1). Taking more realistic values of C to account for the different geometry of dike d0 would only increase our estimates of $\Delta\epsilon$ by a factor 2 [*Boore*, 1977]. The term "average" here implies that values of strain change are averaged over the crack surface.

[69] The average strain change is dimensionless, and can be understood as a displacement-to-length ratio, providing an estimate of how much separation or relative slip of the crack walls occurs for a given crack size. This ratio can be readily used to compare the amount of strain energy released by dikes and earthquakes.

[70] The average stress change associated with diking or earthquake rupture can be deduced from the average strain change in equation (B1) after multiplication by the appropriate elastic modulus: shear modulus μ for earthquakes and Young's modulus E for dikes.

B2. Comparison Between Dikes and Earthquakes

[71] For the dikes studied in this paper, parameters $\tilde{D}$ and S are directly constrained by our inversions, and estimation of the magnitude of the strain change is straightforward. The values of $\tilde{D}$ and S are calculated individually for each dike, by taking into account patches with an opening $D > 0.1\, D_{max}$, where D_{max} is the maximum dike opening. Strain changes deduced in this manner are in the range of $5–50 \times 10^{-5}$. With a Young's modulus of $E = 3 \times 10^{10}$ Pa [*Touloukian*, 1981; *Stein et al.*, 1991], we obtain normal stress changes in the range of 15–150 bars for dikes intruded in 2005–2009 in the Manda Hararo rift.

[72] Because earthquakes represent a means of partially relieving tectonic stresses, the shear stress change coeval to earthquake rupture is called a "stress drop" by seismologists (hereafter noted $\Delta\tau$). Earthquake shear stress drops are commonly estimated directly from the spectral content of radiated seismic waves, which is dependent both on rupture area and average slip [e.g., *Brune*, 1970]. However, this method is not relevant for dikes, which are largely aseismic objects at high frequency, probably due to their very low rupture velocity (~1 km/h for dikes versus >1 km/s for earthquakes) [e.g., *Haskell*, 1964], thus hindering any comparison.

[73] An alternative for calculating average static shear stress drops for earthquakes is to exploit the various scaling laws deduced from study of a large number of earthquakes, which relate geometric and kinematic parameters associated with seismic ruptures, such as the magnitude-length relation [e.g., *Kanamori and Anderson*, 1975; *Romanowicz and Ruff*, 2002; *King and Wesnousky*, 2007]. For instance, *Wells and Coppersmith* [1994] provide an empirical relation between moment magnitude M_w and rupture area S (in m^2) for an

extensive global catalogue of earthquakes of various mechanisms and magnitudes:

$$M_w = -1.81 + 0.98\log(S) \approx -1.81 + 1\log(S) \quad \text{(B2)}$$

[74] Using the definition of the moment magnitude [*Hanks and Kanamori*, 1979],

$$M_w = -6.03 + \frac{2}{3}\log\left(\mu S \tilde{D}\right) \quad \text{(B3)}$$

where μ is the shear modulus (here expressed in Pa), S is the rupture area (in m^2), and $\tilde{D}$ is the mean slip (in m), we deduce that the population of earthquakes following the statistical relation of *Wells and Coppersmith* [1994] corresponds to an average shear stress drop of $\Delta\tau = 21$ bars (using the formula $\Delta\tau = \mu\tilde{D}/\sqrt{S}$). This is the same order of magnitude as the value of 60 bars reported by *Kanamori and Anderson* [1975] and agrees well with several recent compilations of earthquake stress drops [e.g., *Manighetti et al.*, 2007; *Allmann and Shearer*, 2009]. Using a shear modulus of $\mu = 3 \times 10^{10}$ Pa, these values correspond to a shear strain change in the range of $7–20 \times 10^{-5}$ (dashed lines in Figure 7c).

[75] Note that in the above calculations, the values of Young's modulus and shear modulus were chosen to be equal. In fact, the "seismological" shear modulus of $\mu = 3 \times 10^{10}$ Pa is equivalent to a Young's modulus of $E = 7.5 \times 10^{10}$ Pa (using a Poisson ratio of $\nu = 0.25$ and the formula $E = 2\mu\ (1 + \nu)$). The choice of a "reduced" Young's modulus of $E = 3.0 \times 10^{10}$ Pa for stress changes induced by dikes in the Manda Hararo rift is justified by numerous studies carried out in areas of volcanic unrest [e.g., *Gudmundsson*, 1988; *Cayol and Cornet*, 1998], which have shown that the "seismological" Young's modulus is too high, perhaps by as much as one order of magnitude, to reconcile geodetic measurements and pressure changes in magma reservoirs inferred from physical modeling.

[76] **Acknowledgments.** We are grateful to late Pascal Favreau for his encouragements at an early stage of this work. This paper benefited from fruitful discussions with François Beauducel, Cécile Doubre and Benoît Taisne. We thank Arthur Delorme and Geneviève Moguilny, who provided assistance for the InSAR processing. One anonymous reviewer and Stephen J. Martel made constructive remarks that helped improve the manuscript. We thank the European Space Agency (ESA) for programming the Envisat satellite and providing data crucial to this work (AOE-272, AOE-720). The Repeat Orbit Interferometry Package (ROI_PAC) software was provided by Caltech/Jet Propulsion Laboratory (JPL). We acknowledge the contribution of David Bowman in the development of the Marzipan and Nutcracker softwares, which were used for stress calculations. Most figures were prepared with the Generic Mapping Tool (GMT) software [*Wessel and Smith*, 1991]. This is IPGP contribution 3060.

References

Aki, K. (1972), Earthquake mechanism, *Tectonophysics*, *13*, 423–446, doi:10.1016/0040-1951(72)90032-7.

Allmann, B. P., and P. M. Shearer (2009), Global variations of stress drop for moderate to large earthquakes, *J. Geophys. Res.*, *114*, B01310, doi:10.1029/2008JB005821.

Amelung, F., S.-H. Yun, T. R. Walter, P. Segall, and S.-W. Kim (2007), Stress control of deep rift intrusion at Mauna Loa Volcano, Hawaii, *Science*, *316*, 1026–1030, doi:10.1126/science.1140035.

Anderson, E. M. (1938), The dynamics of sheet intrusion, *Proc. R. Soc. Edinburgh*, *58*, 242–251.

Arnott, S. K., and G. R. Foulger (1994), The Krafla spreading segment, Iceland. 2: The accretionary stress cycle and nonshear earthquake focal mechanisms, *J. Geophys. Res.*, *99*, 23,827–23,827, doi:10.1029/94JB00688.

Audin, L., X. Quidelleur, E. Coulié, V. Courtillot, S. Gilder, I. Manighetti, P.-Y. Gillot, P. Tapponnier, and T. Kidane (2004), Palaeomagnetism and K-Ar and $^{40}Ar/^{39}Ar$ ages in the Ali Sabieh area (Republic of Djibouti and Ethiopia): constraints on the mechanism of Aden ridge propagation into southeastern Afar during the last 10 Myr, *Geophys. J. Int.*, *158*, 327–345, doi:10.1111/j.1365-246X.2004.02286.x.

Ayele, A., E. Jacques, M. Kassim, T. Kidane, A. Omar, S. Tait, A. Nercessian, J.-B. de Chabalier, and G. C. P. King (2007), The volcano seismic crisis in Afar, Ethiopia, starting September 2005, *Earth Planet. Sci. Lett.*, *255*, 177–187, doi:10.1016/j.epsl.2006.12.014.

Ayele, A., D. Keir, C. Ebinger, T. J. Wright, G. W. Stuart, W. R. Buck, E. Jacques, G. Ogubazghi, and J. Sholan (2009), September 2005 mega-dike emplacement in the Manda-Harraro nascent oceanic rift (Afar depression), *Geophys. Res. Lett.*, *36*, L20306, doi:10.1029/2009GL039605.

Barberi, F., H. Tazieff, and J. Varet (1972), Volcanism in the Afar depression: Its tectonic and magmatic significance, *Tectonophysics*, *15*, 59–64, doi:10.1016/0040-1951(72)90051-0.

Beauducel, F., P. Briole, and J.-L. Froger (2000), Volcano-wide fringes in ERS synthetic aperture radar interferograms of Etna (1992–1998): Deformation or tropospheric effect?, *J. Geophys. Res.*, *105*(B7), 16,391–16,402, doi:10.1029/2000JB900095.

Belachew, M., C. J. Ebinger, D. Keir, D. M. Cote, and A. Ayele (2009), Comparison of dike intrusions in Afar: Seismic perspective for source and extent, *Eos Trans. AGU*, *90*(52), Fall Meet. Suppl., Abstract T31B-1811.

Berardino, P., G. Fornaro, R. Lanari, and E. Sansosti (2002), A new algorithm for surface deformation monitoring based on small baseline differential SAR interferograms, *IEEE Trans. Geosci. Remote Sens.*, *40*, 2375–2383, doi:10.1109/TGRS.2002.803792.

Berckhemer, H., B. Baier, H. Gebrande, J. Makris, H. Menzel, H. Miller, and R. Vees (1975), Deep seismic soundings in the Afar region and on the highland of Ethiopia, in *Proceedings of an International Symposium on the Afar Region and RiftRelated Problems, Bad Bergzabren, Germany*, edited by A. Pilger and A. RÖsler, pp. 89–107, Schweizerbart, Stuttgart, Germany.

Björnsson, A. (1985), Dynamics of crustal rifting in NE Iceland, *J. Geophys. Res.*, *90*(B12), 10,151–10,162, doi:10.1029/JB090iB12p10151.

Boore, D. M. (1977), Effect of the free surface on calculated stress drops, *Bull. Seismol. Soc. Am.*, *67*(6), 1661–1664.

Brandsdöttir, B., and P. Einarsson (1979), Seismic activity associated with the September 1977 deflation of the Krafla central volcano in northeastern Iceland, *J. Volcanol. Geotherm. Res.*, *6*, 197–212, doi:10.1016/0377-0273(79)90001-5.

Bruce, P. M., and H. E. Huppert (1989), Thermal control of basaltic fissure eruptions, *Nature*, *342*, 665–667, doi:10.1038/342665a0.

Brune, J. N. (1970), Tectonic stress and the spectra of seismic shear waves from earthquakes, *J. Geophys. Res.*, *75*, 4997–5009, doi:10.1029/JB075i026p04997.

Buck, W. R., L. L. Lavier, and A. N. B. Poliakov (2005), Modes of faulting at mid-ocean ridges, *Nature*, *434*, 719–723, doi:10.1038/nature03358.

Buck, W. R., P. Einarsson, and B. Brandsdóttir (2006), Tectonic stress and magma chamber size as controls on dike propagation: Constraints from the 1975–1984 Krafla rifting episode, *J. Geophys. Res.*, *111*(B12), B12404, doi:10.1029/2005JB003879.

Carslaw, H. S., and J. C. Jaeger (1986), *Conduction of Heat in Solids*, 2nd ed., Oxford Univ. Press, New York.

Cavalié, O., M.-P. Doin, C. Lasserre, and P. Briole (2007), Ground motion measurement in the Lake Mead area, Nevada, by differential synthetic aperture radar interferometry time series analysis: Probing the lithosphere rheological structure, *J. Geophys. Res.*, *112*, B03403, doi:10.1029/2006JB004344.

Cayol, V., and F. H. Cornet (1998), Three-dimensional modeling of the 1983–1984 eruption at Piton de la Fournaise Volcano, Réunion Island, *J. Geophys. Res.*, *103*, 18,025–18,037, doi:10.1029/98JB00201.

de Chabalier, J.-B., and J.-P. Avouac (1994), Kinematics of the Asal Rift (Djibouti) determined from the deformation of Fieale Volcano, *Science*, *265*, 1677–1681, doi:10.1126/science.265.5179.1677.

Delaney, P. T., and D. D. Pollard (1981), Deformation of host rocks and flow of magma during growth of minette dikes and breccia bearing intrusions near Ship Rock, New Mexico, *U.S. Geol. Surv. Prof. Pap.*, *1202*, 61 pp.

Doubre, C., I. Manighetti, C. Dorbath, L. Dorbath, E. Jacques, and J. C. Delmond (2007), Crustal structure and magmato-tectonic processes in an active rift (Asal-Ghoubbet, Afar, East Africa): 1. Insights from a 5-month seismological experiment, *J. Geophys. Res.*, *112*, B05405, doi:10.1029/2005JB003940.

Dunn, R. A., V. Lekić, R. S. Detrick, and D. R. Toomey (2005), Three-dimensional seismic structure of the Mid-Atlantic Ridge (35°N): Evidence

for focused melt supply and lower crustal dike injection, *J. Geophys. Res.*, *110*, B09101, doi:10.1029/2004JB003473.

Dziak, R. P., D. K. Smith, D. R. Bohnenstiehl, C. G. Fox, D. Desbruyeres, H. Matsumoto, M. Tolstoy, and D. J. Fornari (2004), Evidence of a recent magma dike intrusion at the slow spreading Lucky Strike segment, Mid-Atlantic Ridge, *J. Geophys. Res.*, *109*, B12102, doi:10.1029/2004JB003141.

Ebinger, C. J., D. Keir, A. Ayele, E. Calais, T. J. Wright, M. Belachew, J. O. S. Hammond, E. Campbell, and W. R. Buck (2008), Capturing magma intrusion and faulting processes during continental rupture: seismicity of the Dabbahu (Afar) rift, *Geophys. J. Int.*, *174*, 1138–1152, doi:10.1111/j.1365-246X.2008.03877.x.

Einarsson, P. (1991), The Krafla rifting episode 1975–1989, in *Náttúra Mývatns* (*The Nature of Lake Mývatn*), edited by A. G. and Á. Einarsson, p. 97–139, Icelandic Nat. Sci. Soc., Reykjav'k, Iceland.

Eshelby, J. D. (1957), The determination of the elastic field of an ellipsoidal inclusion, and related problems, *Proc. R. Soc. London, Ser. A*, *241*, 376–396, doi:10.1098/rspa.1957.0133.

Farr, T. G., and M. Kobrick (2001), The Shuttle Radar Topography Mission, *Eos Trans. AGU*, *82*(47), Fall Meet. Suppl., Abstract G22B-0214.

Ferguson, D. J., T. D. Barnie, D. M. Pyle, C. Oppenheimer, G. Yirgu, E. Lewi, T. Kidane, S. Carn, and I. Hamling (2010), Recent rift-related volcanism in Afar, Ethiopia, *Earth Planet. Sci. Lett.*, *292*(3–4), 409–418, doi:10.1016/j.epsl.2010.02.010.

Fialko, Y. A., and A. M. Rubin (1998), Thermodynamics of lateral dike propagation: Implications for crustal accretion at slow spreading mid-ocean ridges, *J. Geophys. Res.*, *103*, 2501–2514, doi:10.1029/97JB03105.

Gerbault, M., A. Poliakov, and M. Daignières (1998), Prediction of faulting from the theories of elasticity and plasticity: What are the limits?, *J. Struct. Geol.*, *20*, 301–320, doi:10.1016/S0191-8141(97)00089-8.

Goldstein, R. M., H. A. Zebker, and C. L. Werner (1988), Satellite radar interferometry: Two-dimensional phase unwrapping, *Radio Sci.*, *23*, 713–720, doi:10.1029/RS023i004p00713.

Grandin, R., et al. (2009), September 2005 Manda Hararo-Dabbahu rifting event, Afar (Ethiopia): Constraints provided by geodetic data, *J. Geophys. Res.*, *114*, B08404, doi:10.1029/2008JB005843.

Grandin, R., A. Socquet, M.-P. Doin, E. Jacques, J.-B. de Chabalier, and G. C. P. King (2010), Transient rift opening in response to multiple dike injections in the Manda Hararo rift (Afar, Ethiopia) imaged by time-dependent elastic inversion of interferometric synthetic aperture radar data, *J. Geophys. Res.*, *115*, B09403, doi:10.1029/2009JB006883.

Gudmundsson, A. (1986), Formation of crustal magma chambers in Iceland, *Geology*, *14*, 164, doi:10.1130/0091-7613(1986)14<164:FOCMCI>2.0.CO;2.

Gudmundsson, A. (1988), Effect of tensile stress concentration around magma chambers on intrusion and extrusion frequencies, *J. Volcanol. Geotherm. Res.*, *35*, 179–194, doi:10.1016/0377-0273(88)90015-7.

Hamling, I. J., A. Ayele, L. Bennati, E. Calais, C. J. Ebinger, D. Keir, E. Lewi, T. J. Wright, and G. Yirgu (2009), Geodetic observations of the ongoing Dabbahu rifting episode: New dyke intrusions in 2006 and 2007, *Geophys. J. Int.*, *178*, 989–1003, doi:10.1111/j.1365-246X.2009.04163.x.

Hanks, T. C., and H. Kanamori (1979), A moment magnitude scale, *J. Geophys. Res.*, *84*, 2348–2350, doi:10.1029/JB084iB05p02348.

Hannsen, R. F. (2001), *Radar Interferometry: Data Interpretation and Error Analysis*, Springer, Heidelberg, Germany.

Haskell, N. A. (1964), Total energy and energy spectral density of elastic wave radiation from propagating faults, *Bull. Seismol. Soc. Am.*, *54* (6A), 1811–1841.

Hayward, N. J., and C. J. Ebinger (1996), Variations in the along-axis segmentation of the Afar Rift system, *Tectonics*, *15*, 244–257, doi:10.1029/95TC02292.

Jönsson, S., H. Zebker, P. Segall, and F. Amelung (2002), Fault slip distribution of the 1999 M_w 7.1 Hector Mine, California, earthquake, estimated from satellite radar and GPS measurements, *Bull. Seismol. Soc. Am.*, *92*(4), 1377–1389, doi:10.1785/0120000922.

Kanamori, H., and D. L. Anderson (1975), Theoretical basis of some empirical relations in seismology, *Bull. Seismol. Soc. Am.*, *65*(5), 1073–1095.

Keir, D., et al. (2009), Evidence for focused magmatic accretion at segment centers from lateral dike injections captured beneath the Red Sea rift in Afar, *Geology*, *37*(1), 59–62, doi:10.1130/G25147A.1.

King, G. C. P. (2007), Fault interaction, earthquake stress changes, and the evolution of seismicity, in *Treatise on Geophysics*, vol. 4, edited by G. Schubert, pp. 225–255, doi:10.1016/B978-044452748-6.00069-9, Elsevier, Amsterdam.

King, G. C. P., and S. G. Wesnousky (2007), Scaling of fault parameters for continental strike-slip earthquakes, *Bull. Seismol. Soc. Am.*, *97*, 1833–1840, doi:10.1785/0120070048.

Kostrov, B. V., and S. Das (1988), *Principles of Earthquake Source Mechanics*, 286 pp., Cambridge Univ. Press, Cambridge, U. K.

Lahitte, P., P.-Y. Gillot, T. Kidane, V. Courtillot, and A. Bekele (2003), New age constraints on the timing of volcanism in central Afar, in the presence of propagating rifts, *J. Geophys. Res.*, *108*(B2), 2123, doi:10.1029/2001JB001689.

Lin, J., G. M. Purdy, H. Schouten, J.-C. Sempere, and C. Zervas (1990), Evidence from gravity data for focused magmatic accretion along the Mid-Atlantic Ridge, *Nature*, *344*, 627–632, doi:10.1038/344627a0.

Lister, J. R., and R. C. Kerr (1991), Fluid-mechanical models of crack propagation and their application to magma transport in dykes, *J. Geophys. Res.*, *96*, 10,049–10,077, doi:10.1029/91JB00600.

Lohman, R. B., and M. Simons (2005), Some thoughts on the use of InSAR data to constrain models of surface deformation: Noise structure and data downsampling, *Geochem. Geophys. Geosyst.*, *6*, Q01007, doi:10.1029/2004GC000841.

Manighetti, I., P. Tapponnier, V. Courtillot, Y. Gallet, E. Jacques, and P.-Y. Gillot (2001), Strain transfer between disconnected, propagating rifts in Afar, *J. Geophys. Res.*, *106*, 13,613–13,665, doi:10.1029/2000JB900454.

Manighetti, I., M. Campillo, S. Bouley, and F. Cotton (2007), Earthquake scaling, fault segmentation, and structural maturity, *Earth Planet. Sci. Lett.*, *253*, 429–438, doi:10.1016/j.epsl.2006.11.004.

Mastin, L. G., and D. D. Pollard (1988), Surface deformation and shallow dike intrusion processes at Inyo craters, Long Valley, California, *J. Geophys. Res.*, *93*, 13,221–13,235, doi:10.1029/JB093iB11p13221.

McLeod, P., and S. Tait (1999), The growth of dykes from magma chambers, *J. Volcanol. Geotherm. Res.*, *92*, 231–245, doi:10.1016/S0377-0273(99)00053-0.

Mériaux, C., and C. Jaupart (1995), Simple fluid dynamic models of volcanic rift zones, *Earth Planet. Sci. Lett.*, *136*, 223–240, doi:10.1016/0012-821X(95)00170-H.

Nooner, S. L., L. Bennati, E. Calais, W. R. Buck, I. J. Hamling, T. J. Wright, and E. Lewi (2009), Post-rifting relaxation in the Afar region, Ethiopia, *Geophys. Res. Lett.*, *36*, L21308, doi:10.1029/2009GL040502.

Okada, Y. (1985), Surface deformation due to shear and tensile faults in a half space, *Bull. Seismol. Soc. Am.*, *75*(4), 1135–1154.

Okada, Y. (1992), Internal deformation due to shear and tensile faults in a half-space, *Bull. Seismol. Soc. Am.*, *82*(2), 1018–1040.

Pollard, D. D., and P. Segall (1987), Theoretical displacements and stresses near fractures in rock: with applications to faults, joints, veins, dikes, and solution surfaces, in *Fracture Mechanics of Rock*, edited by B. K. Atkinson, pp. 277–349, Academic, London.

Pollard, D. D., P. T. Delaney, W. A. Duffield, E. T. Endo, and A. T. Okamura (1983), Surface deformation in volcanic rift zones, *Tectonophysics*, *94*(1–4), 541–584, doi:10.1016/0040-1951(83)90034-3.

Rivalta, E. (2010), Evidence that coupling to magma chambers controls the volume history and velocity of laterally propagating intrusions, *J. Geophys. Res.*, *115*, B07203, doi:10.1029/2009JB006922.

Romanowicz, B., and L. J. Ruff (2002), On moment-length scaling of large strike slip earthquakes and the strength of faults, *Geophys. Res. Lett.*, *29*(12), 1604, doi:10.1029/2001GL014479.

Rosen, P. A., S. Henley, G. Peltzer, and M. Simons (2004), Updated repeat orbit interferometry package released, *Eos Trans. AGU*, *85*(5), 47, doi:10.1029/2004EO050004.

Rowland, J. V., E. Baker, C. J. Ebinger, D. Keir, T. Kidane, J. Biggs, N. Hayward, and T. J. Wright (2007), Fault growth at a nascent slow-spreading ridge: 2005 Dabbahu rifting episode, Afar, *Geophys. J. Int.*, *171*(3), 1226–1246, doi:10.1111/j.1365-246X.2007.03584.x.

Rubin, A. M. (1990), A comparison of rift-zone tectonics in Iceland and Hawaii, *Bull. Volcanol.*, *52*, 302–319, doi:10.1007/BF00304101.

Rubin, A. M. (1992), Dike-induced faulting and graben subsidence in volcanic rift zones, *J. Geophys. Res.*, *97*(B2), 1839–1858, doi:10.1029/91JB02170.

Rubin, A. M. (1995), Propagation of magma-filled cracks, *Annu. Rev. Earth Planet. Sci.*, *23*, 287–336, doi:10.1146/annurev.ea.23.050195.001443.

Rubin, A. M., and D. D. Pollard (1987), Origins of blade-like dikes in volcanic rift zones, *U.S. Geol. Surv. Prof. Pap.*, *1350*, 1449–1470.

Sæmundsson, K. (1979), Outline of the geology of Iceland, *Joekull*, *29*, 7–28.

Schmidt, D. A., and R. Bürgmann (2003), Time-dependent land uplift and subsidence in the Santa Clara valley, California, from a large interferometric synthetic aperture radar data set, *J. Geophys. Res.*, *108*(B9), 2416, doi:10.1029/2002JB002267.

Scholz, C. H. (2002), *The Mechanics of Earthquakes and Faulting*, 2nd ed., 496 pp., Cambridge Univ. Press, Cambridge, U. K.

Shaw, W. J., and J. Lin (1996), Models of ocean ridge lithospheric deformation: Dependence on crustal thickness, spreading rate, and segmentation, *J. Geophys. Res.*, *101*, 17,977–17,993, doi:10.1029/96JB00949.

Simons, M., and P. A. Rosen (2007), Interferometric synthetic aperture radar, in *Treatise on Geophysics*, vol. 3, edited by G. Schubert, pp. 391–446, doi:10.1016/B978-044452748-6.00059-6, Elsevier, Amsterdam.

Smith, D. K., and J. R. Cann (1999), Constructing the upper crust of the Mid-Atlantic Ridge: A reinterpretation based on the Puna Ridge, Kilauea Volcano, *J. Geophys. Res.*, *104*, 25,379–25,399, doi:10.1029/1999JB900177.

Stein, R. S., P. Briole, J.-C. Ruegg, P. Tapponnier, and F. Gasse (1991), Contemporary, holocene, and quaternary deformation of the Asal rift, Djibouti: Implications for the mechanics of slow spreading ridges, *J. Geophys. Res.*, *96*, 21,789–21,806, doi:10.1029/91JB02118.

Takada, A. (1989), Magma transport and reservoir formation by a system of propagating cracks, *Bull. Volcanol.*, *52*(2), 118–126, doi:10.1007/BF00301551.

Tarantola, A., and B. Valette (1982), Generalized nonlinear inverse problems solved using the least squares criterion, *Rev. Geophys.*, *20*, 219–232, doi:10.1029/RG020i002p00219.

Touloukian, Y. S. (1981), *Physical Properties of Rocks and Minerals*, McGraw-Hill, New York.

Turcotte, D. L., and G. Shubert (1982), *Geodynamics: Applications of Continuum Physics to Geological Problems*, John Wiley, New York.

Varet, J. (1975), Geological map of Central Afar, Cent. Natl. de la Res. Sci., Paris.

Varet, J., and F. Gasse (1978), Géologie de l'Afar Central et Méridional, Cent. Natl. de la Res. Sci., Paris.

Weertman, J. (1971), Theory of water-filled crevasses in glaciers applied to vertical magma transport beneath oceanic ridges, *J. Geophys. Res.*, *76*(5), 1171–1183, doi:10.1029/JB076i005p01171.

Wells, D. L., and K. J. Coppersmith (1994), New empirical relationships among magnitude, rupture length, rupture width, rupture area, and surface displacement, *Bull. Seismol. Soc. Am.*, *84*(4), 974–1002.

Wessel, P., and W. H. F. Smith (1991), Free software helps map and display data, *Eos Trans. AGU*, *72*, 441, doi:10.1029/90EO00319.

Wills, S., and W. R. Buck (1997), Stress-field rotation and rooted detachment faults: A Coulomb failure analysis, *J. Geophys. Res.*, *102*, 20,503–20,514, doi:10.1029/97JB01512.

Wright, R., L. P. Flynn, H. Garbeil, A. J. L. Harris, and E. Pilger (2004), MODVOLC: Near-real-time thermal monitoring of global volcanism, *J. Volcanol. Geotherm. Res.*, *135*, 29–49, doi:10.1016/j.jvolgeores.2003.12.008.

Wright, T. J., C. Ebinger, J. Biggs, A. Ayele, G. J. Yirgu, D. Keir, and A. Stork (2006), Magma-maintained rift segmentation at continental rupture in the 2005 Afar dyking episode, *Nature*, *442*, 291–294, doi:10.1038/nature04978.

Yirgu, G., A. Ayele, and D. Ayalew (2006), Recent seismovolcanic crisis in northern Afar, Ethiopia, *Eos Trans. AGU*, *87*(33), 325–329, doi:10.1029/2006EO330001.

Yirgu, G., A. Ayele, S. Fisseha, T. Chernet, K. Damtew, and S. Carn (2007), Manda Hararo: First historical eruption lava flows–SO_2 plume from rift fissure–August 2007, *Bull. Global Volcanism Network*, *32*(7).

Zandbergen, R., P. Righetti, M. Otten, D. Kuijper, and J. Dow (2002), Routine operational and high-precision orbit determination of Envisat, paper presented at 34th COSPAR Scientific Assembly, COSPAR, Houston, Tex.

J.-B. de Chabalier, E. Jacques, G. C. P. King, N. Mazzoni, and A. Socquet, Institut de Physique du Globe de Paris, Equipe de Tectonique et Mécanique de la Lithosphère, CNRS UMR 7154, 4 place Jussieu, F-75252 Paris CEDEX 05, France. (dechabal@ipgp.jussieu.fr; jacques@ipgp.jussieu.fr; king@ipgp.jussieu.fr; nelly_mazzoni@yahoo.fr; socquet@ipgp.jussieu.fr)

R. Grandin, Laboratoire de Géologie, École Normale Supérieure, CNRS UMR 8538, 24 Rue Lhmond, F-75231 Paris CEDEX 05, France. (grandin@ipgp.fr)